NASA TECHNICAL NOTE

NASA TN D-5219

c.1

NASA TN D-5219

STATIC LONGITUDINAL AERODYNAMIC CHARACTERISTICS OF SOME SUPERSONIC DECELERATOR MODELS AT MACH NUMBERS OF 2.30 AND 4.63

by Edwin E. Davenport

Langley Research Center
Langley Station, Hampton, Va.

NATIONAL AERONAUTICS AND SPACE ADMINISTRATION • WASHINGTON, D. C. • MAY 1969

STATIC LONGITUDINAL AERODYNAMIC CHARACTERISTICS OF SOME SUPERSONIC DECELERATOR MODELS AT MACH NUMBERS OF 2.30 AND 4.63

By Edwin E. Davenport

Langley Research Center
Langley Station, Hampton, Va.

NATIONAL AERONAUTICS AND SPACE ADMINISTRATION

For sale by the Clearinghouse for Federal Scientific and Technical Information
Springfield, Virginia 22151 – CFSTI price $3.00

STATIC LONGITUDINAL AERODYNAMIC CHARACTERISTICS OF SOME SUPERSONIC DECELERATOR MODELS AT MACH NUMBERS OF 2.30 AND 4.63

By Edwin E. Davenport
Langley Research Center

SUMMARY

An experimental investigation of spherically blunted 120° cones, tension shell models, and a model representative of an attached inflatable decelerator (AID) has been conducted by the National Aeronautics and Space Administration at Mach numbers of 2.30 and 4.63 through an angle-of-attack range from about -5° to about 20°.

The results showed a reduction in axial force with an increase in shoulder radius for the cone models. Good agreement between theoretical and experimental values of standoff distance and bow-wave shape was obtained for the 120° cone models at Mach 4.63. The tension shell models produced a higher level of axial-force coefficients than did the cone models. After inflation the attached inflatable decelerator model produced about twice the axial-force coefficient of the cone models.

INTRODUCTION

The planetary entry programs currently being considered by the National Aeronautics and Space Administration involve the development of a vehicle capable of entering a low-density atmosphere, such as that of Mars, and eventually of landing a scientific payload (refs. 1 and 2). Preliminary studies show that an atmospheric-entry configuration with a low ballistic coefficient can utilize aerodynamic deceleration prior to actuation of terminal deceleration devices, such as parachutes or retrorockets, with an appreciable saving in system weight. In addition to the high-drag characteristic, the atmospheric-entry configuration must have inherent aerodynamic stability and should be relatively light in weight.

Two configuration concepts being considered for possible entry vehicles are the blunted cone and the tension shell. Some static aerodynamic characteristics of a series of conical models have been reported in references 3 and 4. The tension shell configuration is designed to minimize weight by the maximum use of structural materials in tension as reported in reference 3. The tension shell configuration has been the subject of

structural studies such as those of reference 5 and of some static aerodynamic tests such as those of references 3 and 6. In addition to these two basic configuration concepts, further consideration of the cone application has led to development of an attached inflatable decelerator (AID) configuration wherein the payload is contained in a rigid conical nose section with an attached inflatable afterbody which is deployed after initial deceleration by the rigid conical nose. The results of drop tests of a large-scale inflated configuration and the results of wind-tunnel tests of scaled inflated AID models are included in reference 7.

A full-scale flight version of either the cone configuration or the tension shell configuration would require a finite base shoulder radius to accommodate structural members and to facilitate fabrication. In addition, both configurations would require some nose bluntness to minimize heating effects and to accommodate ablation surfaces necessary for an atmospheric entry.

Wind-tunnel tests, therefore, have been made to determine some of the effects on the static longitudinal aerodynamic characteristics of varying the base shoulder for a 120° cone configuration and of varying the nose radius for a tension shell configuration having a constant shoulder radius. In addition, the static longitudinal aerodynamic characteristics were determined for a configuration having a 120° cone forebody and a simulated attached inflatable decelerator (AID) afterbody. Presented herein are the results of these tests which were made in the Langley Unitary Plan wind tunnel at Mach numbers of 2.30 and 4.63 through an angle-of-attack range from about -5° to about 20°.

SYMBOLS

Measurements for this investigation are given in the International System of Units (SI). Equivalent values in U.S. Customary Units are presented within parentheses. Details concerning the use of SI and the physical constants and conversion factors are given in reference 8.

The aerodynamic coefficients are referred to the body system of axes shown in the following sketch which indicates the positive direction of forces and moments:

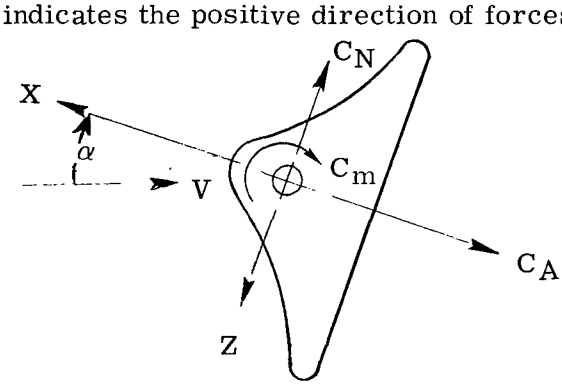

The body-axis system for each model originates at the center-of-moment position shown in figure 1.

A^2	shape parameter for tension shell configurations as defined in reference 5
C_A	axial-force coefficient, $\frac{\text{Axial force}}{qS}$
C_m	pitching-moment coefficient, $\frac{\text{Pitching moment}}{qSd}$
C_N	normal-force coefficient, $\frac{\text{Normal force}}{qS}$
d	maximum model diameter, 20.32 centimeters (8.00 in.)
M	free-stream Mach number
q	free-stream dynamic pressure, newtons/meter^2 (lb/ft^2)
R	Reynolds number
r_b	base radius
r_n	nose radius
r_s	shoulder radius
S	model base area, $\frac{\pi d^2}{4}$
x,r	longitudinal and radial coordinates
α	angle of attack, degrees

APPARATUS

Models

Details of the models are given in figure 1, and photographs of the models are presented as figure 2. All the models were machined from 2024-T4 aluminum alloy and had the same base diameter. The surfaces exposed to the airstream were polished and aerodynamically smooth.

As can be seen in figure 2(a), the spherically blunted 120° cone models were fitted with split interchangeable aftersections to provide shoulder-to-base radius ratios r_s/r_b of 0, 0.025 (not shown), 0.05, 0.10, 0.20, 0.30, and 0.40. A nose radius of $0.20r_b$ was provided for the first four aftersections and the aftersection having $r_s/r_b = 0.40$. A nose section with $r_n/r_b = 0.25$ was provided for the aftersections having shoulder radii of $0.20r_b$, $0.30r_b$, and $0.40r_b$.

The coordinates for the tension shell models are given in figure 1 and this shape represents the basic contour defined by $A^2 = 0.833$. The mathematical derivation of the parameter A^2 is given in detail in reference 5, where it is shown to be a function of the Newtonian pressure distribution, the dynamic pressure, and the tension stress. An increase in the parameter A^2 results in an increase in body length and a reduction in surface cavity on the cusped or flared portion of the model. Three tension shell configurations having $r_n/r_b = 0.20$, 0.30, and 0.40 and constant shoulder radius were used (fig. 2(b)).

The coordinates for the AID model are also given in figure 1, and a discussion of the theoretical shape determination is presented in reference 7. The AID model of the present investigation (fig. 2(c)) had design proportions similar to those of one of the earlier models discussed in reference 7 but did not incorporate the base cavity or a burble fence in its design.

Wind Tunnel

The models were mounted on a sting-supported internal-strain-gage balance in test section number 2 of the Langley Unitary Plan wind tunnel. The wind tunnel is of the variable-pressure, return-flow type and has a test section about 1.2 meters square (4 feet) and about 2.1 meters long (7 feet). The nozzle leading to the test section is of the asymmetric sliding-block type and can be used to vary the Mach number from about 2.30 to 4.63. Further details of the wind tunnel may be found in reference 9.

TESTS AND ACCURACY

The models were tested at Mach numbers of 2.30 and 4.63 through an angle-of-attack range from about -5° to about 20° at zero sideslip. At Mach 2.30, the Reynolds number was 0.73×10^6 with $q = 11\,826$ N/m^2 (247 psf); at Mach 4.63, the Reynolds number was 0.73×10^6 with $q = 6032$ N/m^2 (126 psf) and 2.01×10^6 with $q = 16\,758$ N/m^2 (350 psf). These test conditions were maintained for both the 120° cones and tension shell models. The AID model was not tested at the higher Reynolds number for Mach 4.63. Stagnation temperature was held at 339° K (150° F) for the tests at $M = 2.30$ and at 353° K (175° F) for the tests at $M = 4.63$. Stagnation dewpoint was maintained at about 239° K (-30° F) to avoid any significant condensation effects in the test section.

The 120° cone model with a nose-to-base radius ratio r_n/r_b of 0.20 was tested with aftersections having r_s/r_b = 0, 0.025, 0.50, 0.10, and 0.40. The 120° cone model with r_n/r_b = 0.25 was tested with aftersections having r_s/r_b = 0.20, 0.30, and 0.40. The tension shell models tested had r_n/r_b = 0.20, 0.30, and 0.40. No artificial roughness was used, and the model surfaces exposed to the airstream were aerodynamically smooth.

The angles of attack, corrected for tunnel flow angularity and sting deflection under aerodynamic load, are estimated to be accurate within ±0.1, and the free-stream Mach numbers of 2.30 and 4.63 are estimated to be accurate within ±0.02 and ±0.05, respectively. The values of C_A presented are gross values which have not been corrected for base pressures. On the basis of wind-tunnel calibrations and of 0.5 percent of the design loads of the strain-gage-balance components, the probable errors in the measured data are estimated to be as follows:

	M = 2.30	M = 4.63	
	$R = 0.73 \times 10^6$	$R = 0.73 \times 10^6$	$R = 2.01 \times 10^6$
C_A	±0.02	±0.03	±0.01
C_N	±0.02	±0.03	±0.01
C_m	±0.006	±0.01	±0.004

RESULTS AND DISCUSSION

120° Cone Configuration

The primary purpose of testing the 120° cone models was to determine the effects of varying shoulder radius on the static aerodynamic characteristics with special emphasis on the relative efficiency of the decelerator. The results show that the axial-force coefficient C_A remained essentially constant with increase in angle of attack up to about 5° for all cone configurations for both test Mach numbers of 2.30 and 4.63 (fig. 3). The axial-force coefficient decreased throughout the angle-of-attack range with increase in r_s/r_b for all values of shoulder radii. At constant values of r_n/r_b, C_A at $\alpha = 0°$ decreased linearly with increase in r_s/r_b as shown in the summary plot of figure 4. The effects of changes in Reynolds number were small but noticeable and changes in Mach number were minor. The effects of an increase in r_n/r_b from 0.20 to 0.25 were negligible as predicted in reference 10.

The models were statically stable about the trim angle of attack ($\alpha = 0°$) for all test conditions (fig. 3). Generally the variation of pitching-moment coefficient C_m with α was relatively insensitive to changes in r_s/r_b. However, the normal-force coefficient C_N at values of α greater than 5° and of r_s/r_b greater than 0.10 increased appreciably as r_s/r_b increased. The center of moments for all models was chosen

to correspond to the base surface of the sharp-shoulder cone to give a common reference for all models.

Typical schlieren photographs of the 120° cone models at $\alpha \approx 0^{\circ}$ are presented as figure 5. In figure 6 an interesting comparison is presented between the experimentally determined bow-wave shapes and shock standoff distance mechanically transposed from enlargements of the photographs of figure 5 for $M = 4.63$ and the approximate numerical results from a computer program which employs the one-strip Belotserkovskii integral method. This program is an unpublished modification of the one described in reference 10, which treated blunt bodies with sharp sonic corners $\left(r_s/r_b = 0\right)$. When the sonic point occurs at a sharp corner, the velocity gradient is infinite there; such singular behavior was accounted for in the method of reference 10. In the present studies, when $r_s/r_b \neq 0$, the transition of the surface velocity through sonic speed occurs on the rounded shoulder, and the velocity gradient at the sonic point is finite (although steep when r_s/r_b is small). The program was modified appropriately to treat the "smooth" sonic point condition, and the procedure is similar to those described in references 11 and 12. The accuracy of the one-strip approximation deteriorates with decreasing Mach number, and $M = 2.30$ was given in reference 10 as the lower limit of applicability for a flat-faced cylinder with $r_s/r_b = 0$. For the blunt cone with rounded shoulder, the quality of the one-strip solution is poor or meaningless at $M = 2.30$, especially in the shoulder region beyond the junction curvature discontinuity. As can be seen in figure 6 for $M = 4.63$ and $r_s/r_b = 0$ to 0.20, the agreement is good. For the shapes studied herein there was little variation in shock standoff distance with change in shoulder radius. Conversely, the shock standoff distance is found to vary almost linearly with r_s/r_b for a flat-faced cylinder (ref. 13).

Tension Shell Configuration

The tension shell models produced a fairly constant level of C_A over an α range from about -5° to 5° for all test conditions as can be seen in figure 7. The configuration with $r_n/r_b = 0.30$ generally had higher values of C_A than the other two models, but values for all models agreed within approximately 3 percent.

The axial-force coefficients at $\alpha \approx 0^{\circ}$ as a function of r_n/r_b for all three tension shell models are summarized in figure 8. The data show a small but noticeable effect of both Mach number and Reynolds number on the drag of the tension shell models. A comparison of figure 8 with figure 4 shows that the tension shell models clearly produced higher drag values at $\alpha \approx 0^{\circ}$ than did the 120° cone models.

The slopes of the curves of C_m as a function of α show that the tension shell configurations were statically stable about the trim angle of attack $(\alpha = 0^{\circ})$ at Mach 2.30 but were marginally stable at Mach 4.63. (See fig. 7.) Variations in C_m and C_N due

to change in nose radius were slight except at the lower Reynolds number of 0.73×10^6 at $M = 4.63$ for α greater than 10^o (fig. 7(b)). Typical schlieren photographs of the tension shell models at $\alpha \approx 0^o$ are presented as figure 9.

Attached Inflatable Decelerator Configuration

The static longitudinal aerodynamic characteristics of a model representative of an attached inflatable decelerator (AID) are presented in figure 10. (As mentioned previously, this model had design proportions similar to those of one of the earlier flight configurations described in reference 7 but did not incorporate the base cavity or burble fence.) The AID model also produced a fairly constant level of C_A for angles of attack from about -4^o to 5^o. An increase in Mach number produced a reduction in the level of C_A but had little or no effect on C_m or C_N. Both normal-force- and pitching-moment-coefficient curves are linear throughout the angle-of-attack range, and the negative slope of the pitching-moment-coefficient curve indicated positive static stability about the trim angle of attack.

In figure 11 the advantage that can be gained by using the attached inflatable decelerator is illustrated. The axial-force-coefficient values shown at the top of the figure are based upon what would be the base area of the hard-shell nose portion prior to inflation of the afterbody (as indicated by the hatched area). Values of C_A at the bottom of the figure are for a sharp-shoulder 120^o cone. The values of C_A at $\alpha = 0^o$ for the AID are more than double the corresponding values for the solid 120^o cone. The much smaller hard-shell nose portion of the AID could possibly eliminate the need for hammerheading in a packaged missile or space-vehicle assembly.

CONCLUSIONS

An experimental investigation of the static longitudinal aerodynamic characteristics of spherically blunted 120^o cones with varied shoulder radii, tension shell models with varied nose radii, and a model representative of an attached inflatable deceleration (AID) was made at Mach numbers of 2.30 and 4.63 for an angle-of-attack range from about -5^o to about 20^o. The following conclusions are indicated:

(1) The 120^o cone models exhibited a reduction in axial force with an increase in shoulder radius throughout the angle-of-attack range.

(2) Good agreement was obtained between theoretically and experimentally determined bow-wave shape and standoff distance for the 120^o cone models for various shoulder radii at Mach 4.63.

(3) The tension shell models exhibited less than a 3-percent change in axial force for the various nose radii and produced higher values of axial force than did the 120° cone.

(4) After inflation the AID model was shown to be capable of producing about twice the axial-force coefficient as a solid cone.

Langley Research Center,
National Aeronautics and Space Administration,
Langley Station, Hampton, Va., March 19, 1969,
124-07-02-67-23.

REFERENCES

1. Pickering, William H.: Mariner 4's Flight to Mars. Astronaut. Aeronaut., vol. 3, no. 10, Oct. 1965, pp. 20-21.

2. Roberts, Leonard: Entry Into Planetary Atmospheres. Astronaut. Aeronaut., vol. 2, no. 10, Oct. 1964, pp. 22-29.

3. Harris, Charles D.: Transonic Aerodynamic Investigation of Tension Shell and Blunted 100° Conical Shapes for Unmanned Entry Vehicles. NASA TN D-3700, 1966.

4. Campbell, James F.; and Howell, Dorothy T.: Supersonic Aerodynamics of Large-Angle Cones. NASA TN D-4719, 1968.

5. Anderson, Melvin S.; Robinson, James C.; Bush, Harold G.; and Fralich, Robert W.: A Tension Shell Structure for Application to Entry Vehicles. NASA TN D-2675, 1965.

6. Deveikis, William D.; and Sawyer, James Wayne: Aerodynamic Characteristics of Tension Shell Shapes at Mach 3.0. NASA TN D-3633, 1966.

7. Mikulas, Martin M., Jr.; and Bohon, Herman L.: Summary of the Development Status of Attached Inflatable Decelerators. AIAA Paper No. 68-929, Sept. 1968.

8. Mechtly, E. A.: The International System of Units – Physical Constants and Conversion Factors. NASA SP-7012, 1964.

9. Schaefer, William T., Jr.: Characteristics of Major Active Wind Tunnels at the Langley Research Center. NASA TM X-1130, 1965.

10. South, Jerry C., Jr.: Calculation of Axisymmetric Supersonic Flow Past Blunt Bodies With Sonic Corners, Including a Program Description and Listing. NASA TN D-4563, 1968.

11. Traugott, Stephen C.: An Approximate Solution of the Direct Supersonic Blunt-Body Problem for Arbitrary Axisymmetric Shapes. J. Aerosp. Sci., vol. 27, no. 5, May 1960, pp. 361-370.

12. Xerikos, J.; and Anderson, W. A.: A Critical Study of the Direct Blunt Body Integral Method. Rep. SM-42603, Missile & Space Syst. Div., Douglas Aircraft Co., Inc., Dec. 28, 1962.

13. Inouye, Mamoru; Marvin, Joseph G.; and Sinclair, A. Richard: Comparison of Experimental and Theoretical Shock Shapes and Pressure Distributions on Flat-Faced Cylinders at Mach 10.5. NASA TN D-4397, 1968.

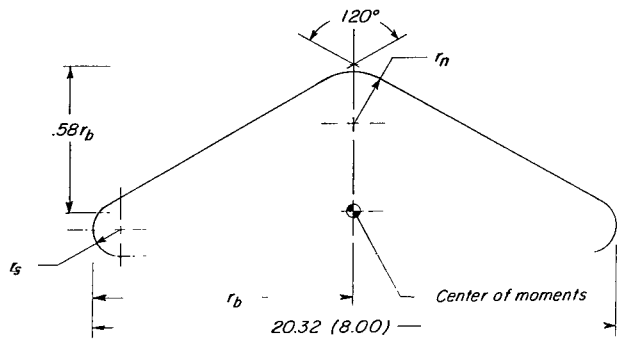

120° cone

Combinations

$\frac{r_s}{r_b}$	$\frac{r_n}{r_b}$
0	.200
.025	.200
.050	.200
.100	.200
.200	.250
.300	.250
.400	.250
.400	.200

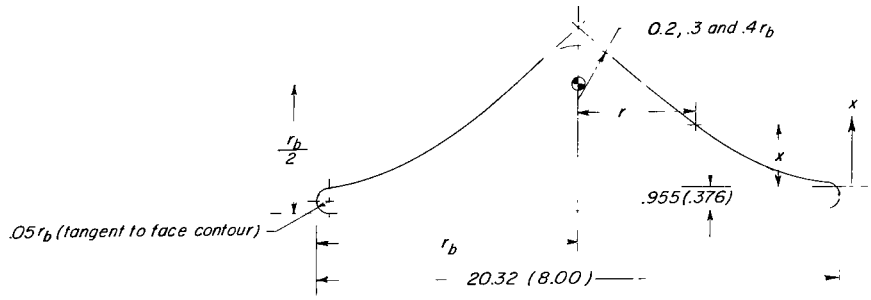

Tension shell

Coordinates

$\frac{x}{r_b}$	$\frac{r}{r_b}$
0.6301	0
.5835	.05
.5372	.10
.4463	.20
.4022	.25
.3594	.30
.3180	.35
.2784	.40
.2406	.45
.2050	.50
.1716	.55
.1407	.60
.1124	.65
.0869	.70
.0643	.75
.0448	.80
.0285	.85
.0155	.90
.0059	.95
0	1.00

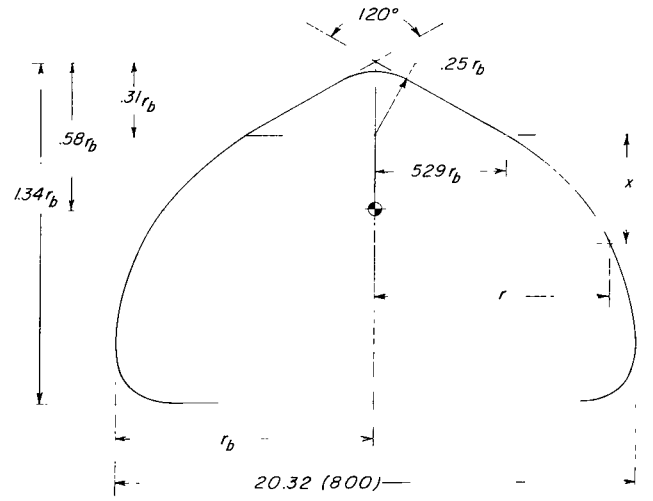

Attached inflatable decelerator

Coordinates

x/r_b	r/r_b
0	0.529
0.092	.646
.183	.728
.275	.804
.361	.866
.458	.910
.549	.947
.641	.974
.732	.995
.824	1.000
.915	.974
1.005	.894
1.037	.688

Figure 1.- Details of models. Linear dimensions are in centimeters (inches).

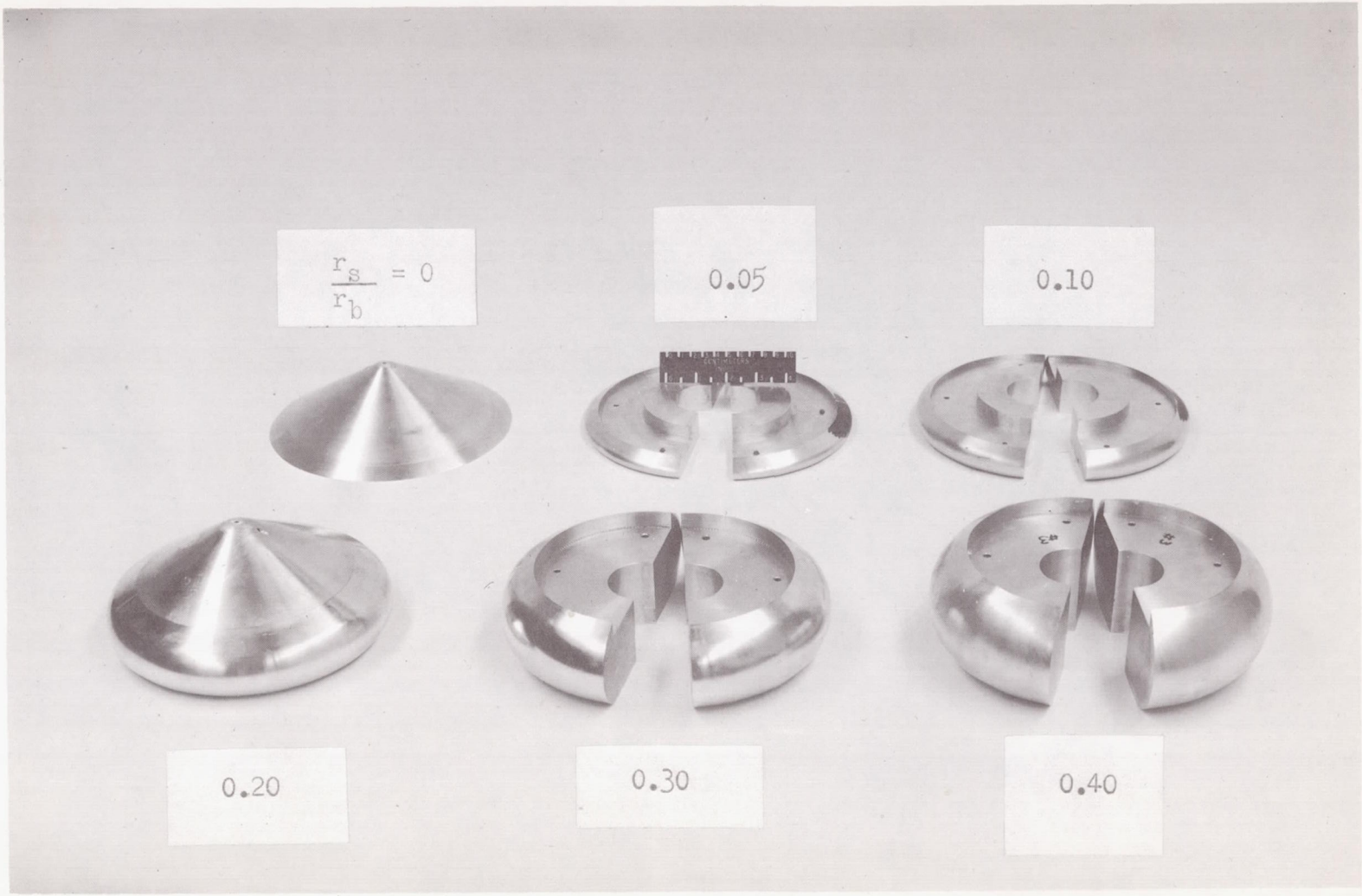

(a) Spherically blunted 120° cones.

L-67-5444.1

Figure 2.- Models used in the investigation.

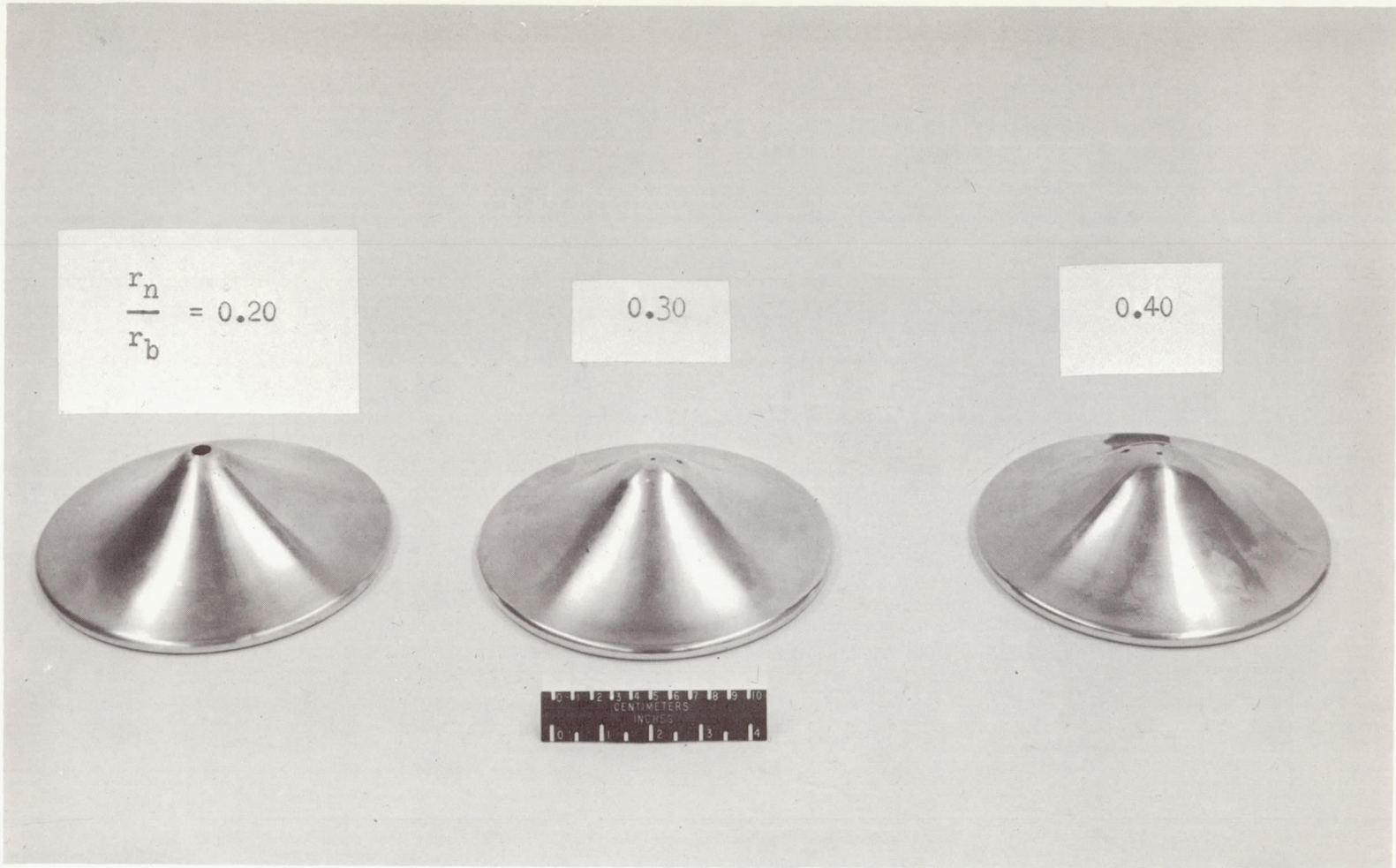

(b) Tension shells.

L-67-5446.1

Figure 2.- Continued.

(c) Attached inflatable decelerator (AID). L-67-5445

Figure 2.- Concluded.

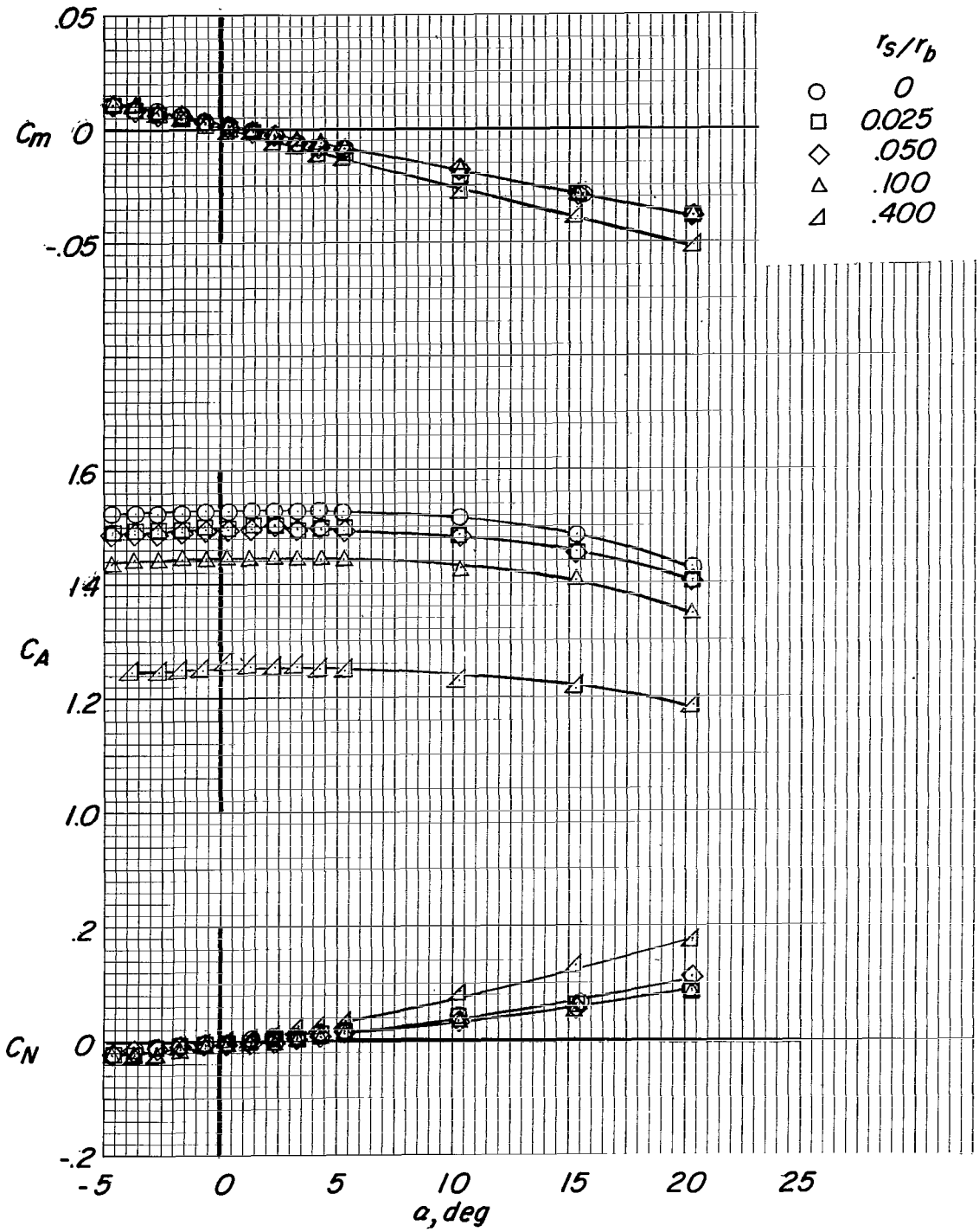

(a) $r_n/r_b = 0.20$; M = 2.30; R = 0.73×10^6.

Figure 3.- Effect of shoulder radius on static longitudinal aerodynamic characteristics of 120^0 cones.

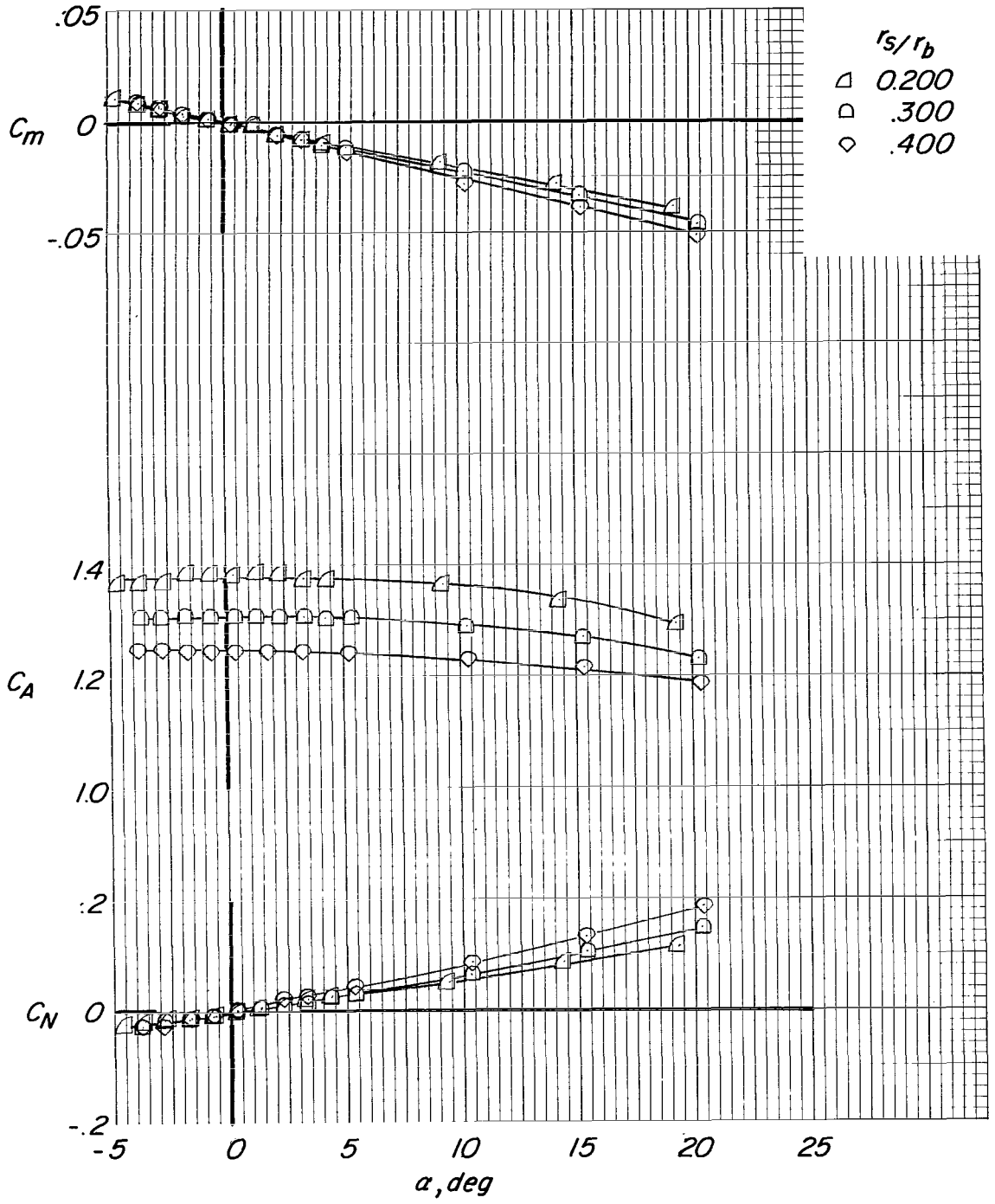

(b) r_n/r_b = 0.25; M = 2.30; R = 0.73 × 10^6.

Figure 3.- Continued.

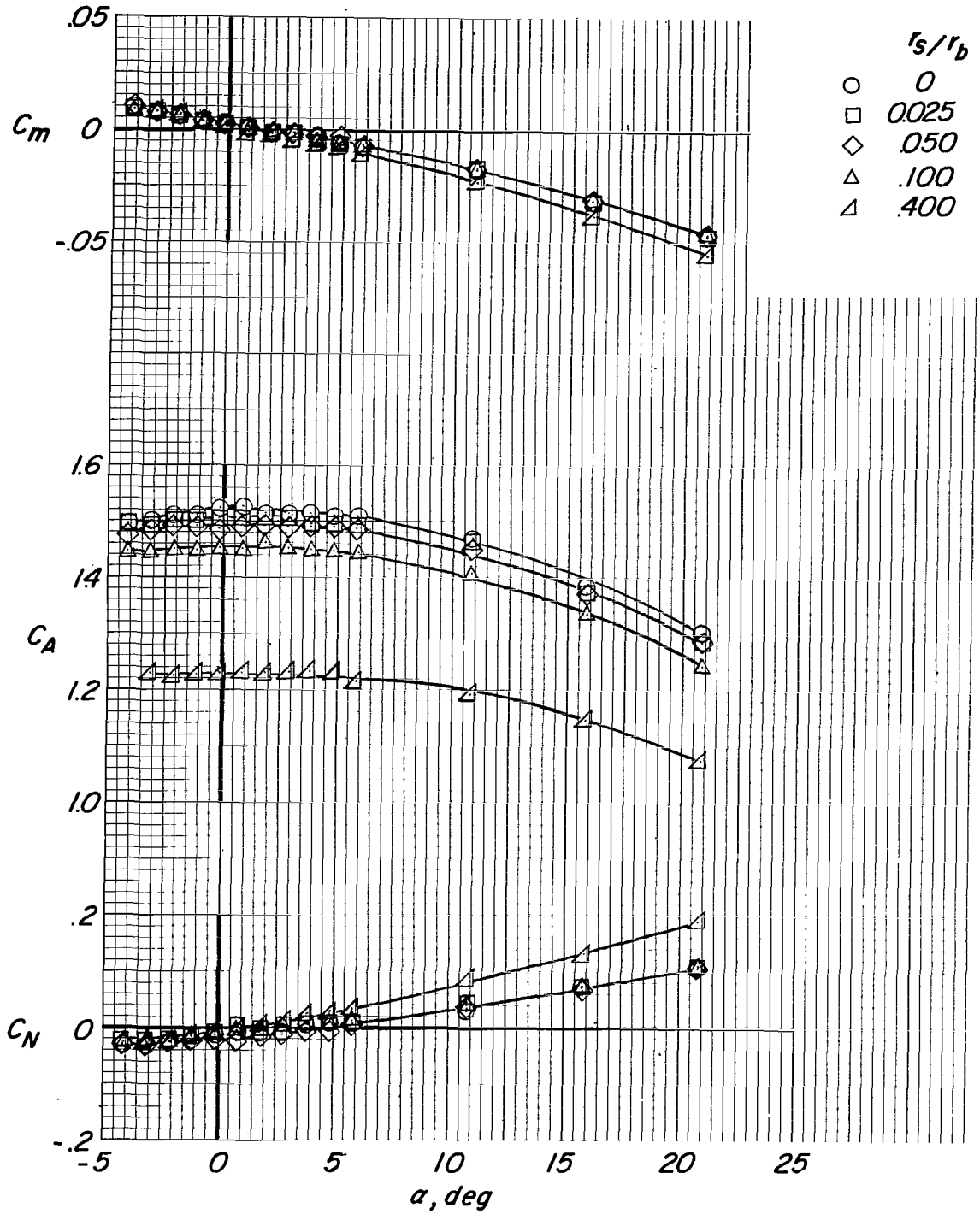

(c) $r_n/r_b = 0.20$; M = 4.63; R = 0.73×10^6.

Figure 3.- Continued.

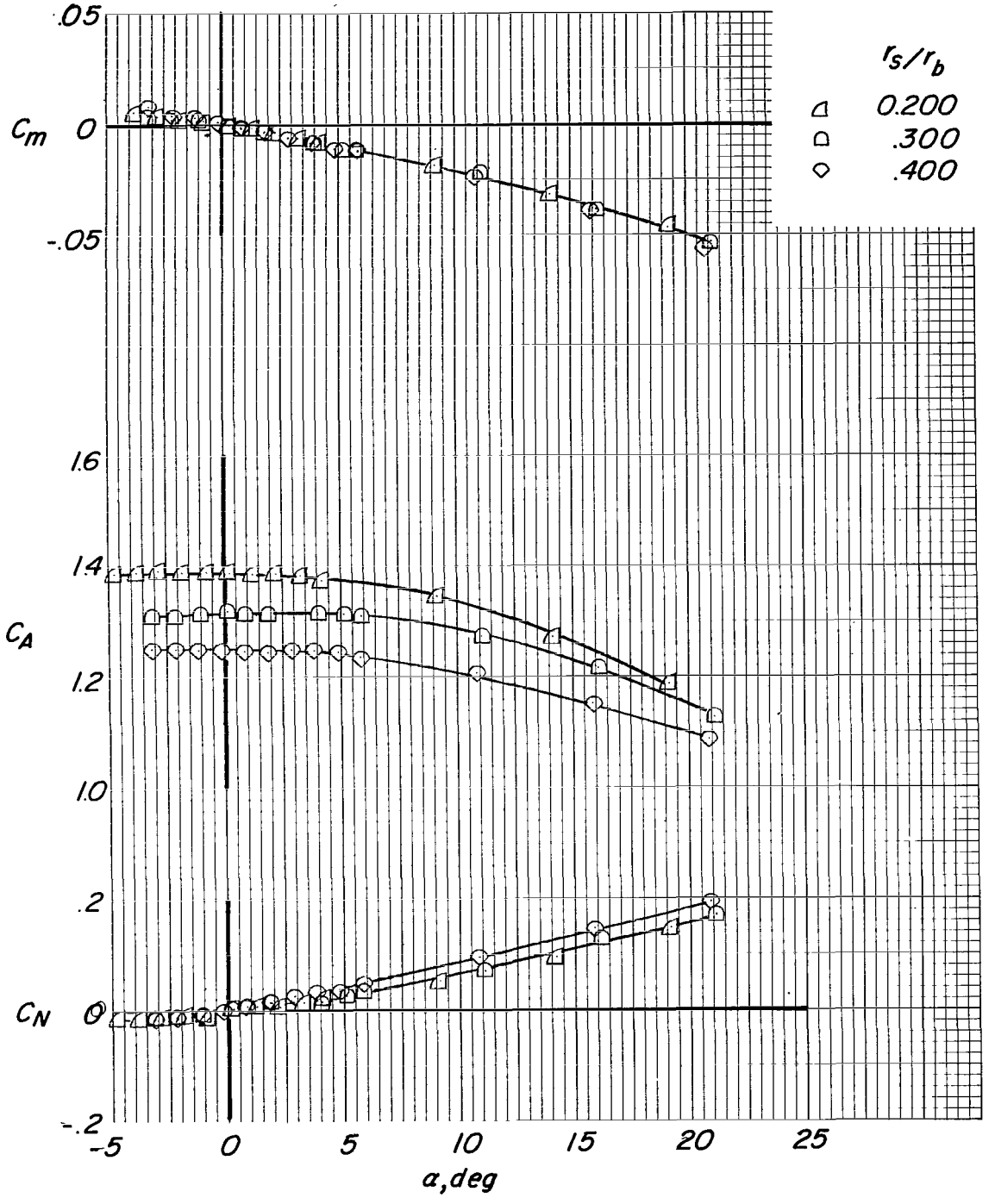

(d) $r_n/r_b = 0.25$; M = 4.63; R = 0.73 × 10^6.

Figure 3.- Continued.

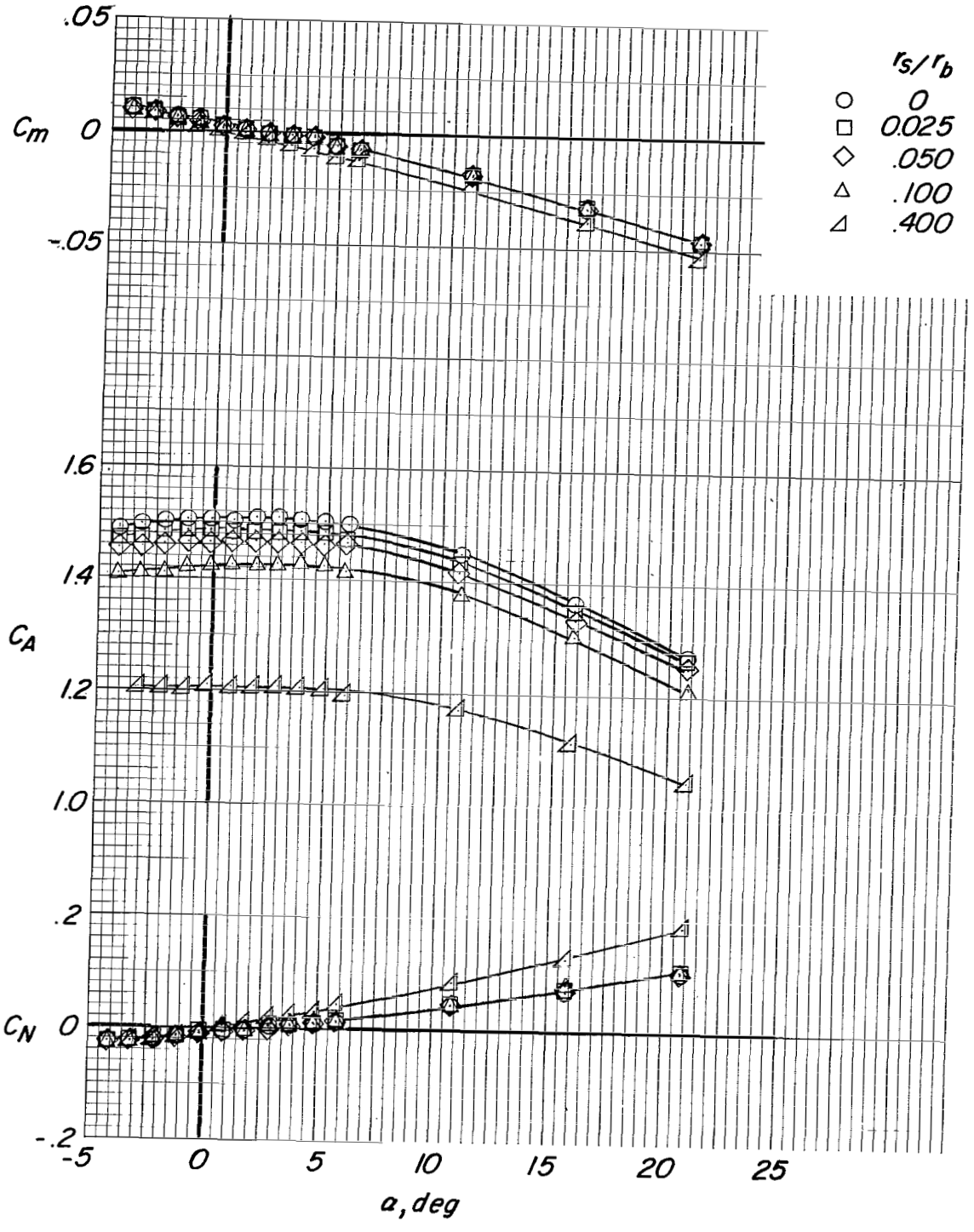

(e) $r_n/r_b = 0.20$; M = 4.63; R = 2.01×10^6.

Figure 3.- Continued.

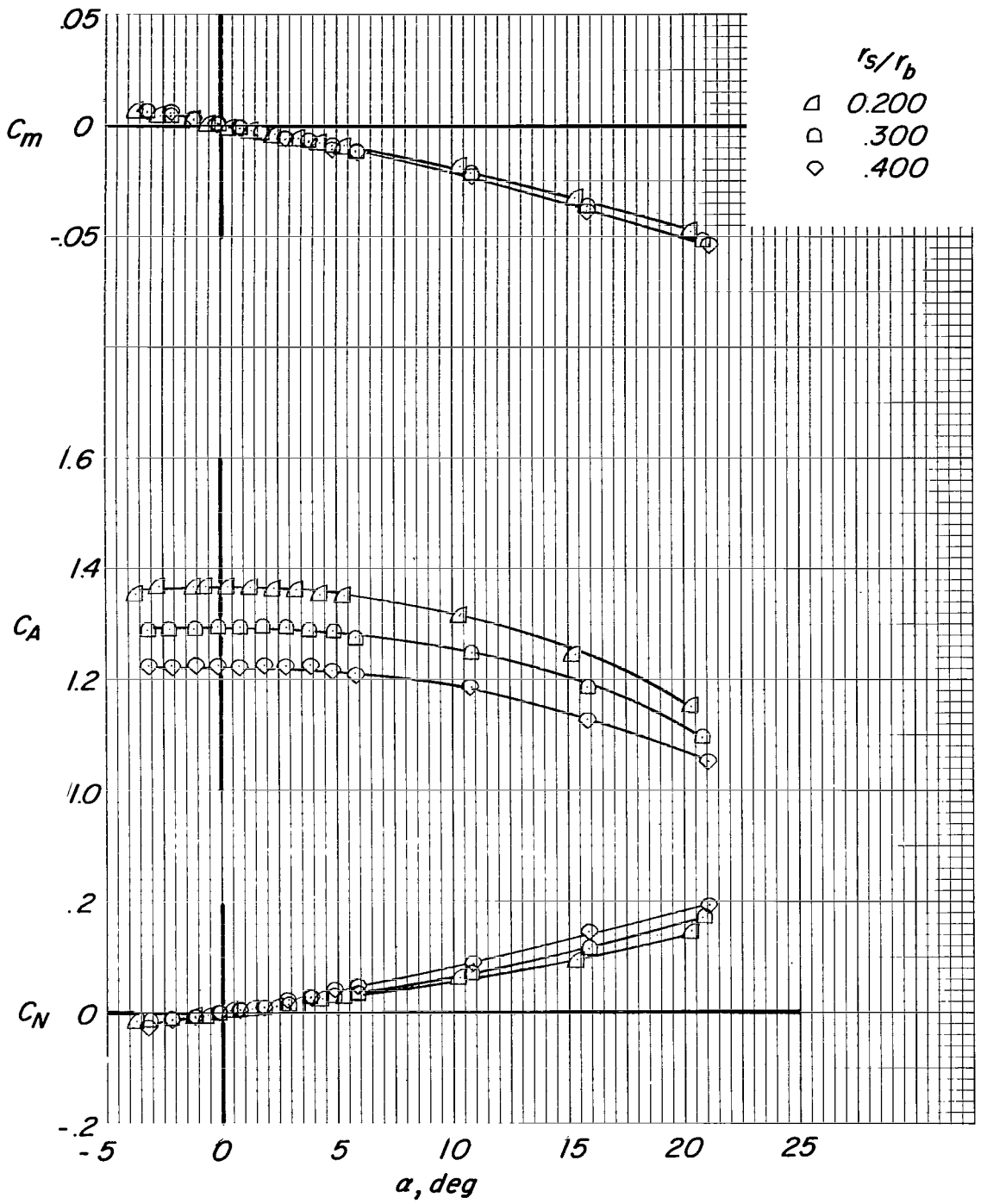

(f) $r_n/r_b = 0.25$; M = 4.63; R = 2.01×10^6.

Figure 3.- Concluded.

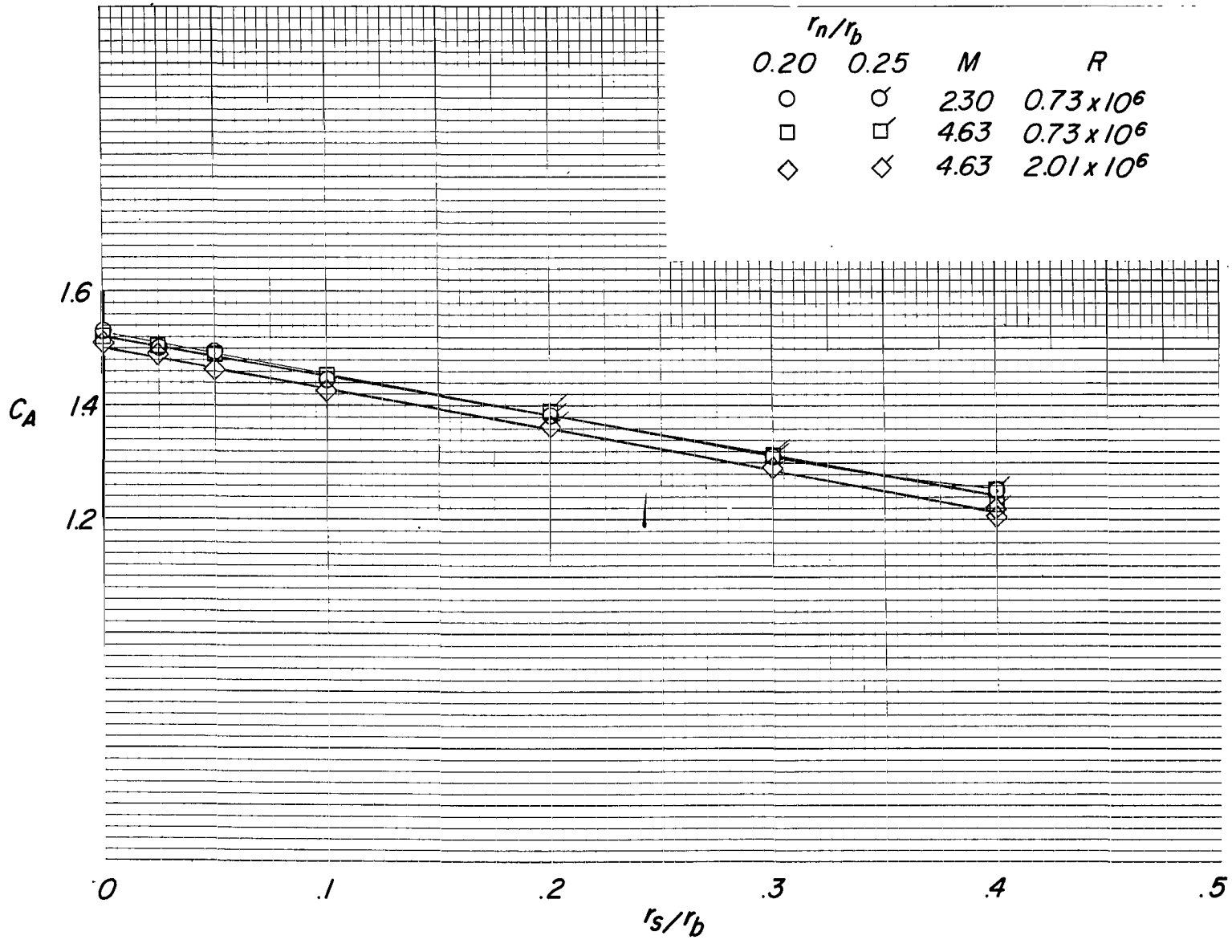

Figure 4.- Summary of axial-force coefficients at $\alpha \approx 0^0$ of 120^0 cones.

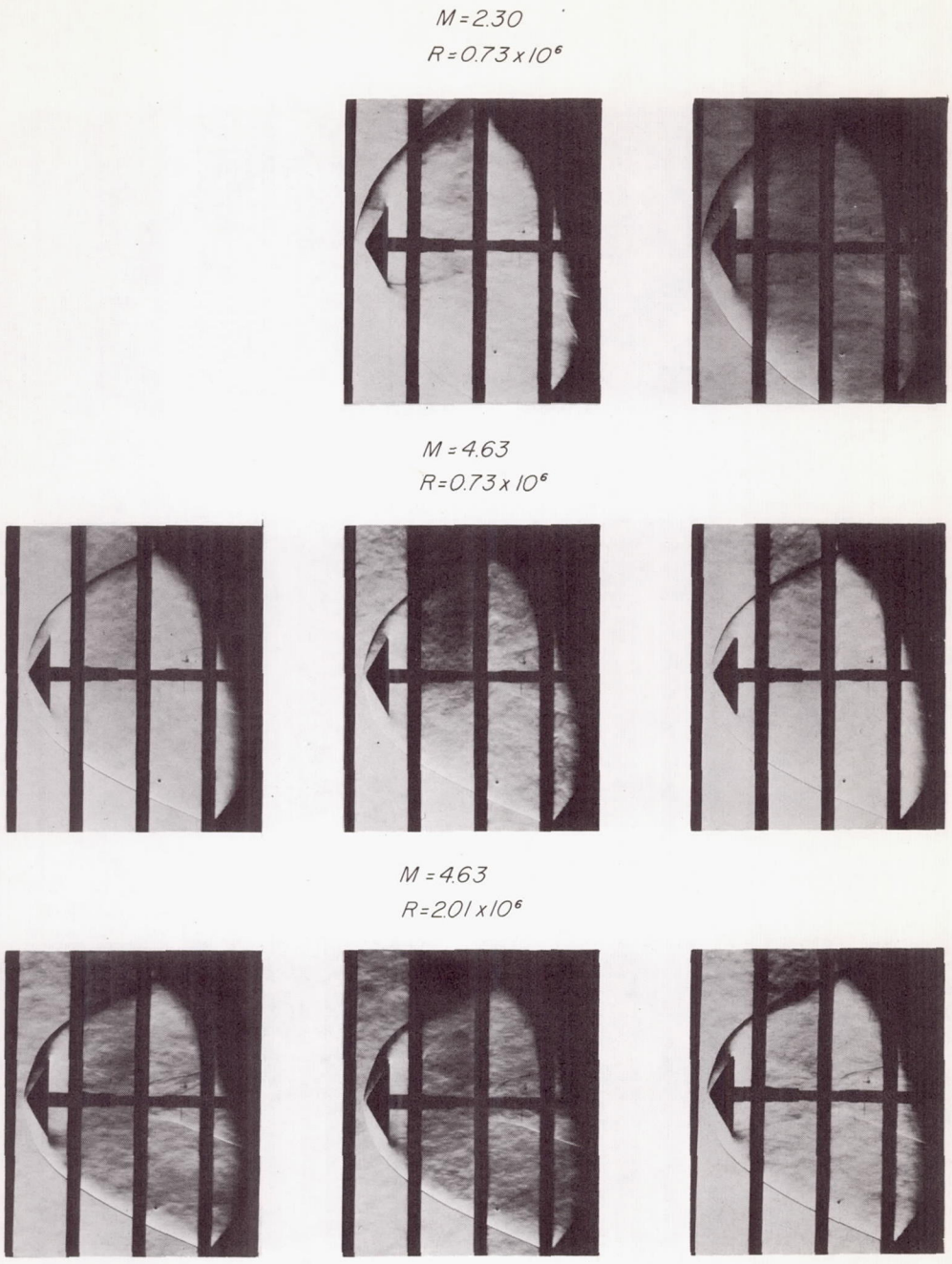

Figure 5.- Schlieren photographs of 120° cones. $\alpha \approx 0^{\circ}$.

L-69-1303

M = 2.30
R = 0.73 x 10^6

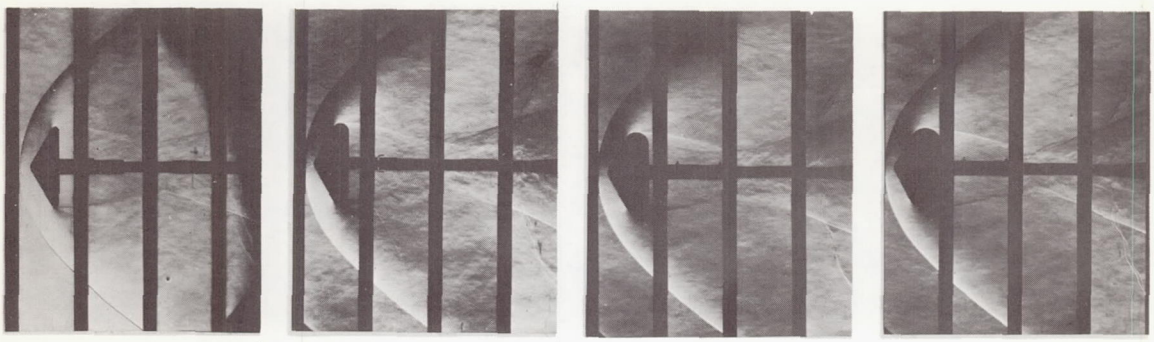

M = 4.63
R = 0.73 x 10^6

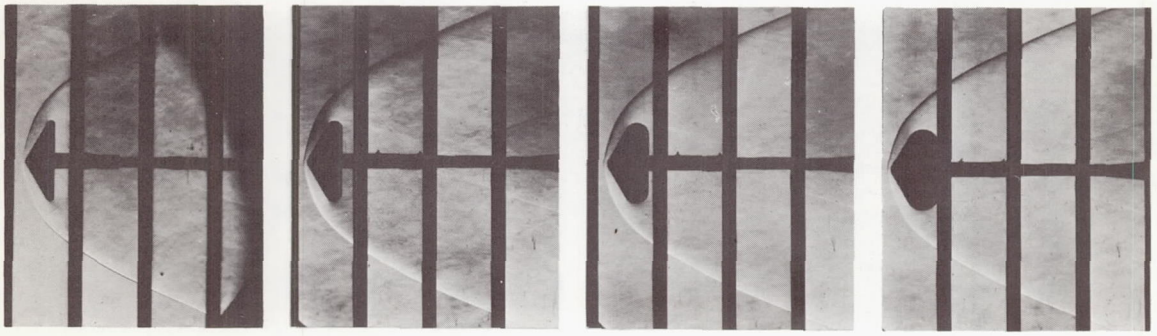

M = 4.63
R = 2.01 x 10^6

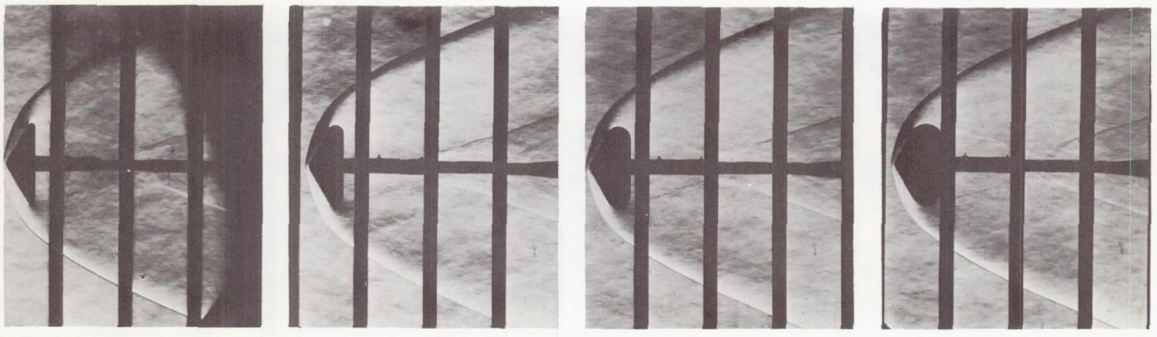

$\frac{r_s}{r_b}$ = 0.10	0.20	0.30	0.40
$\frac{r_n}{r_b}$ = 0.20	0.25	0.25	0.25

Figure 5.- Concluded.

L-69-1304

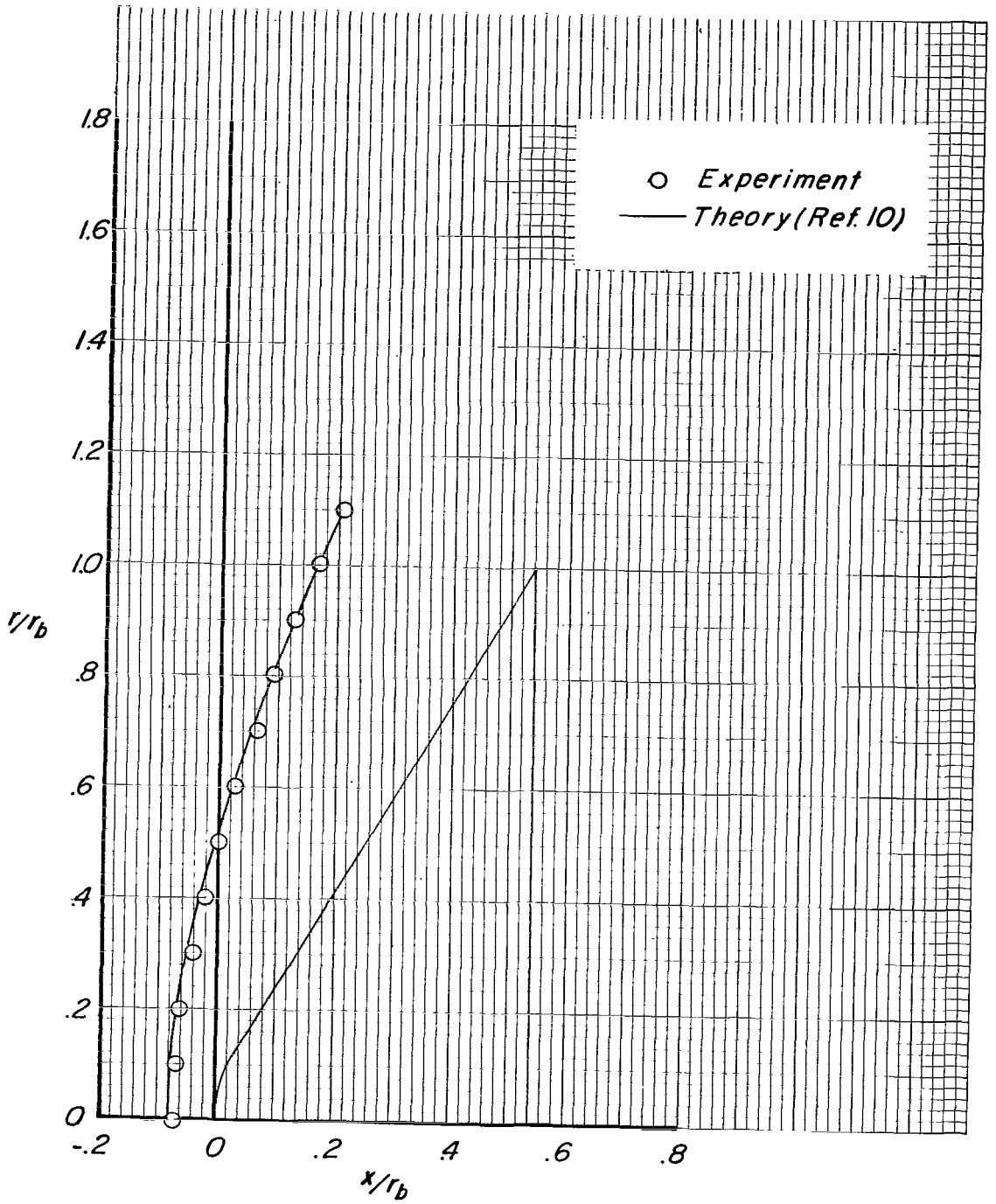

(a) $r_s/r_b = 0$; $r_n/r_b = 0.20$.

Figure 6.- Shock-wave shapes for 120^0 cones. $M = 4.63$; $\alpha \approx 0^0$; $R = 2.01 \times 10^6$.

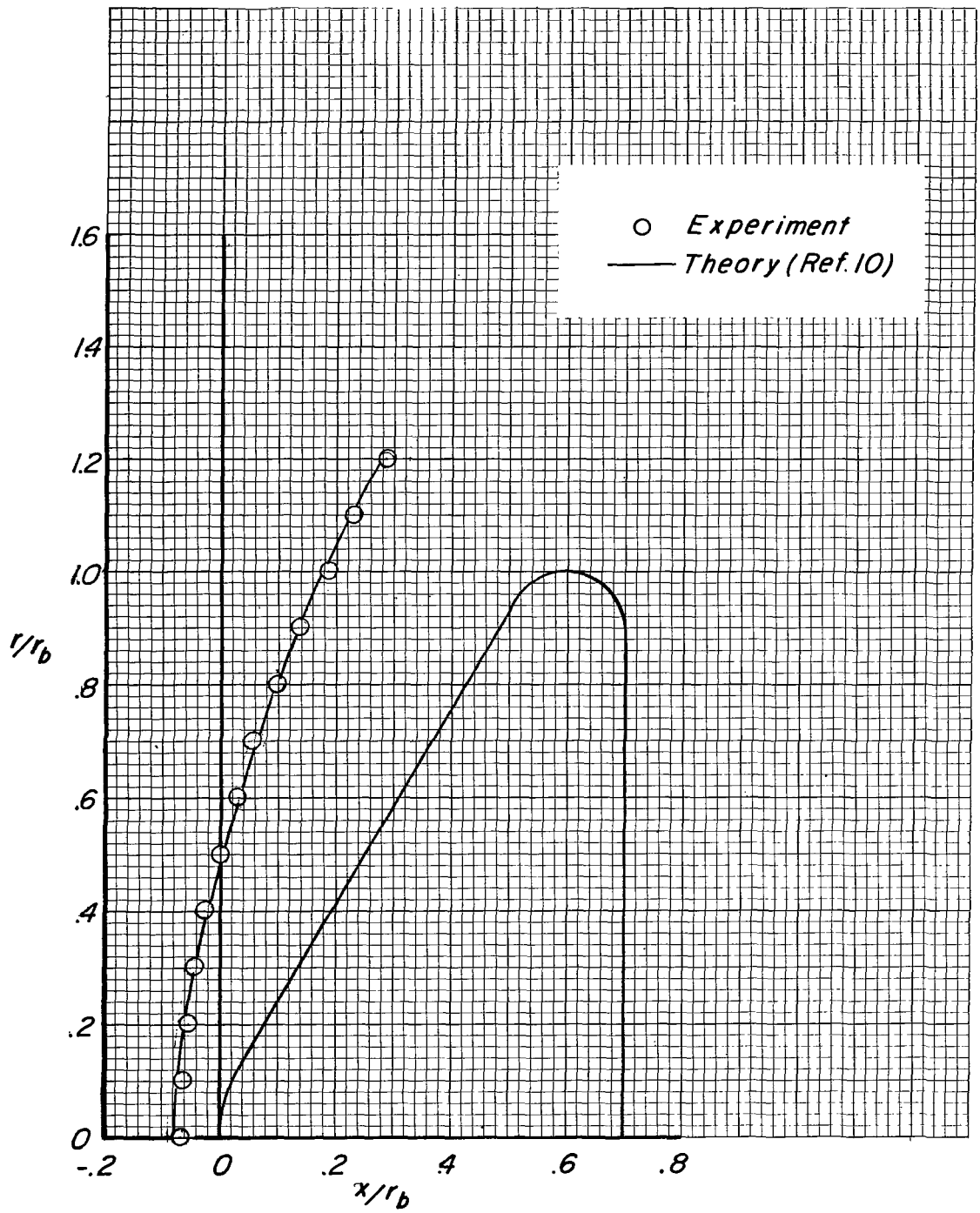

(b) $r_s/r_b = 0.10$; $r_n/r_b = 0.20$.

Figure 6.- Continued.

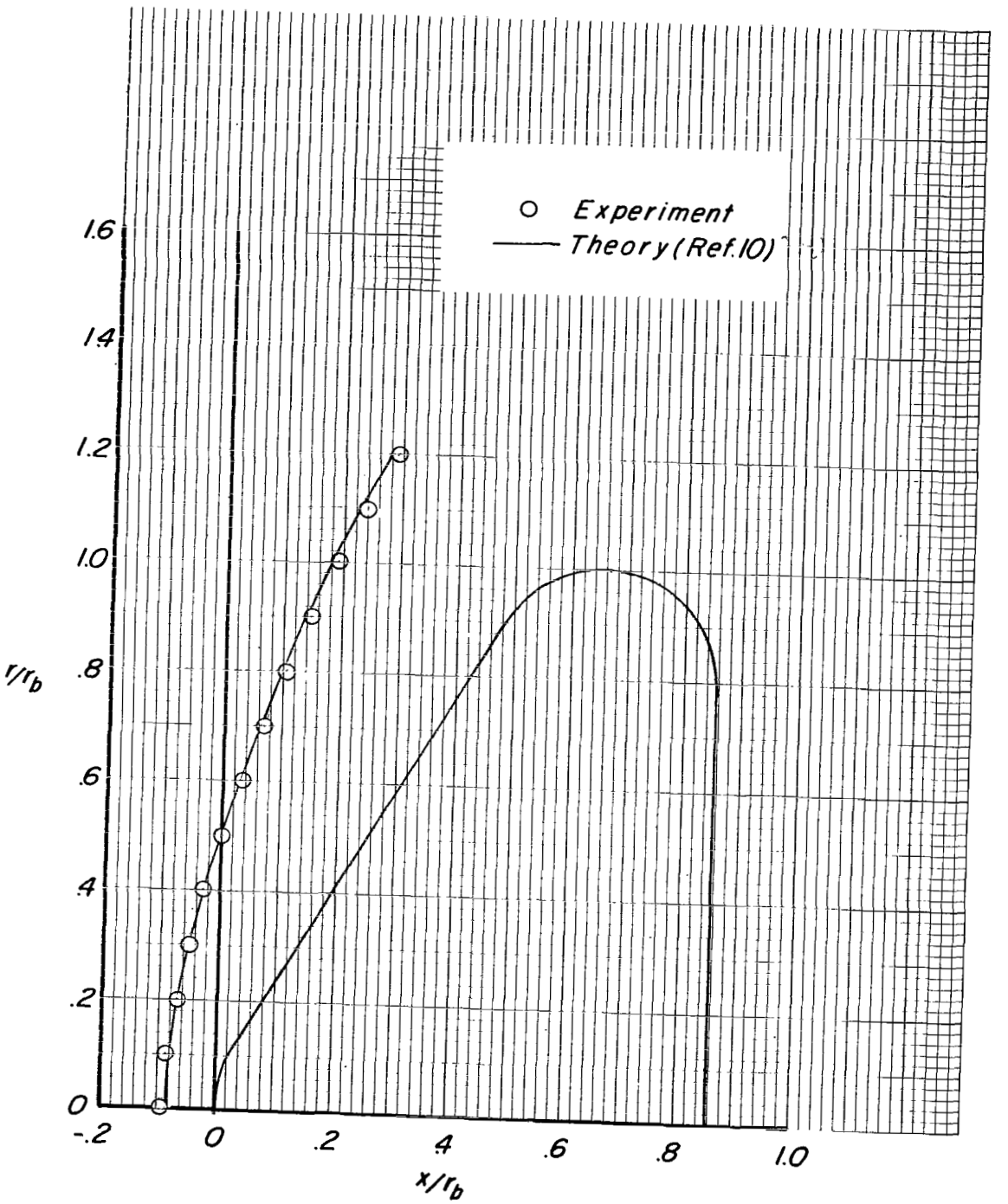

(c) $r_s/r_b = 0.20$; $r_n/r_b = 0.25$.

Figure 6.- Continued.

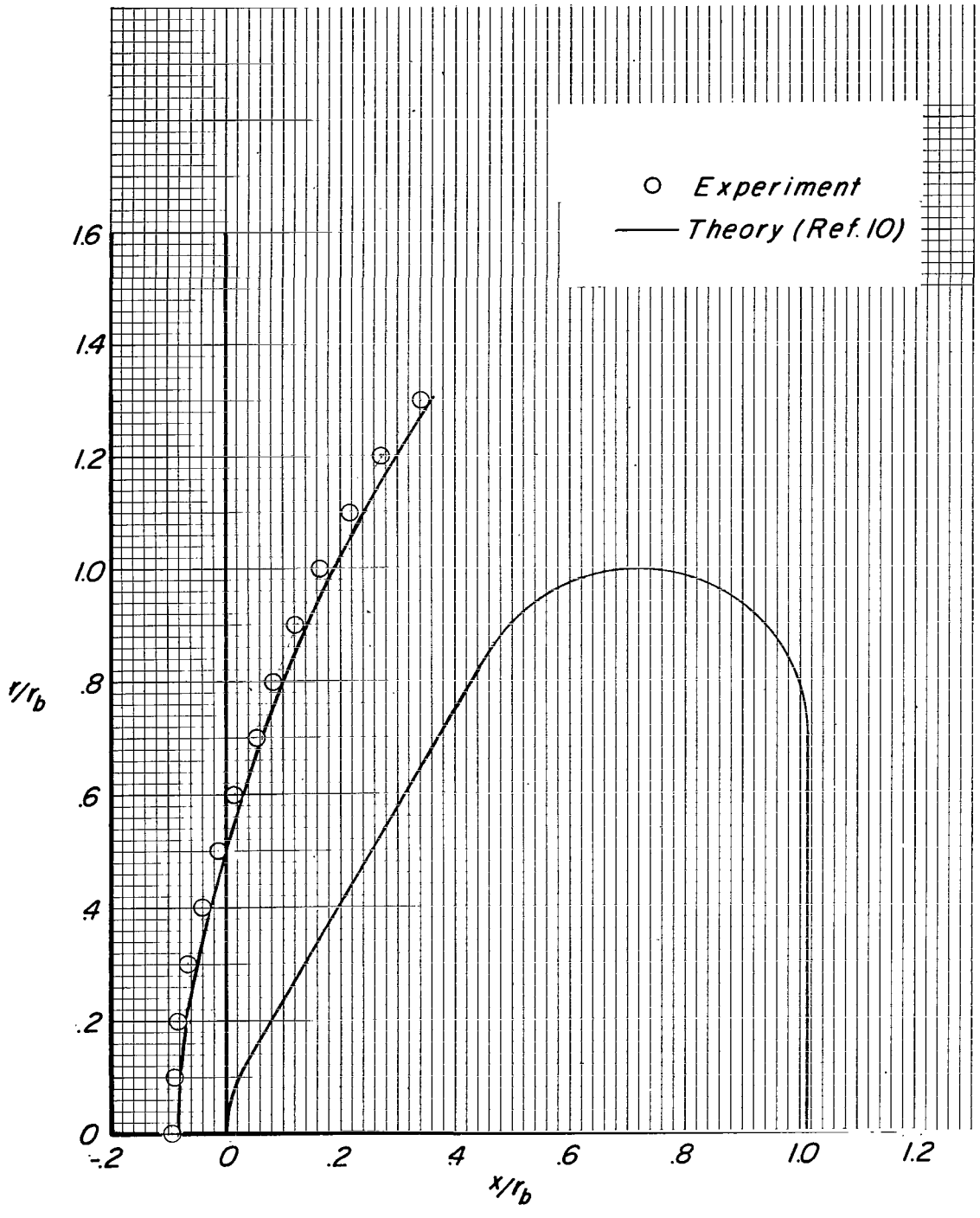

(d) $r_s/r_b = 0.30$; $r_n/r_b = 0.25$.

Figure 6.- Continued.

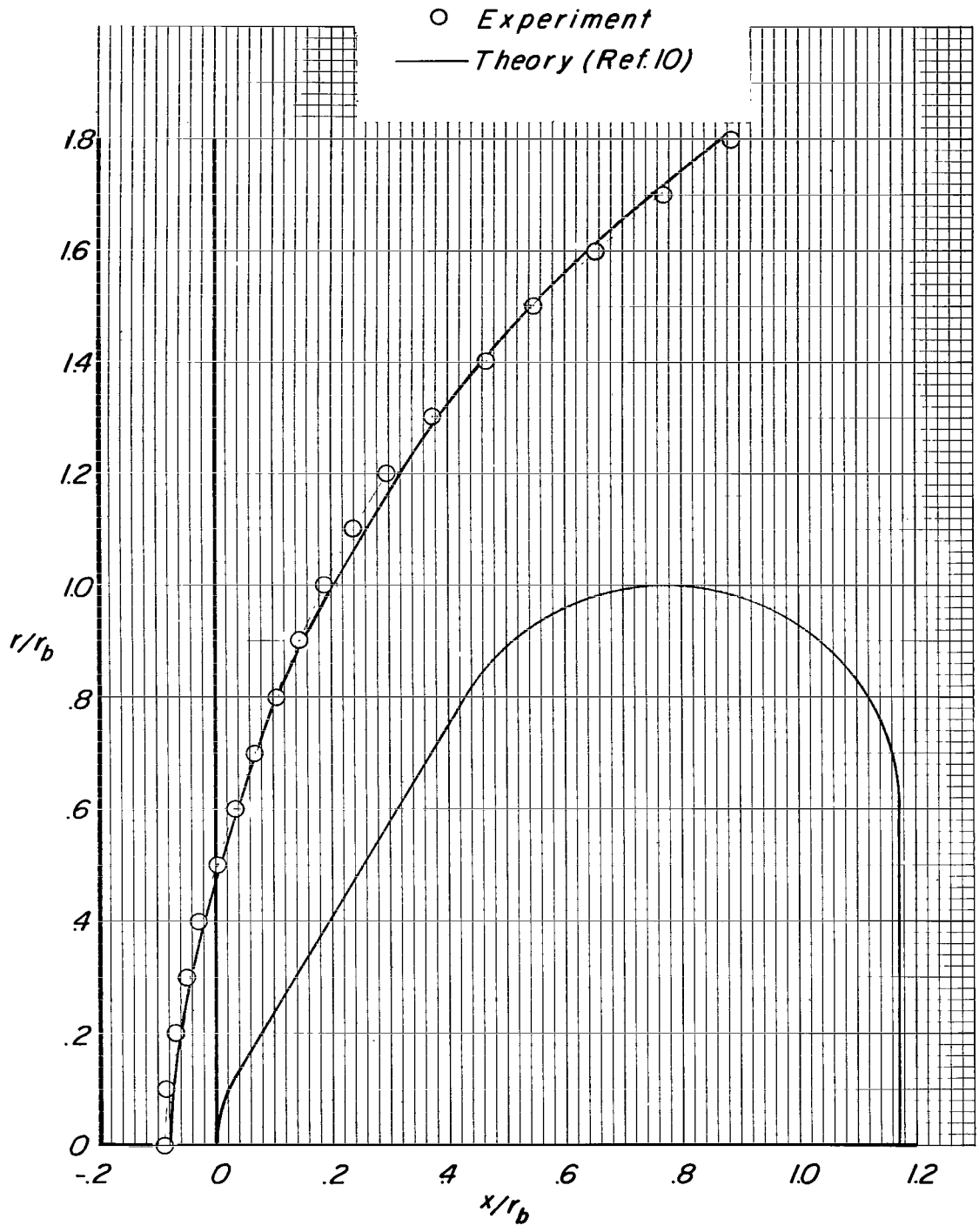

(e) $r_s/r_b = 0.40$; $r_n/r_b = 0.25$.

Figure 6.- Concluded.

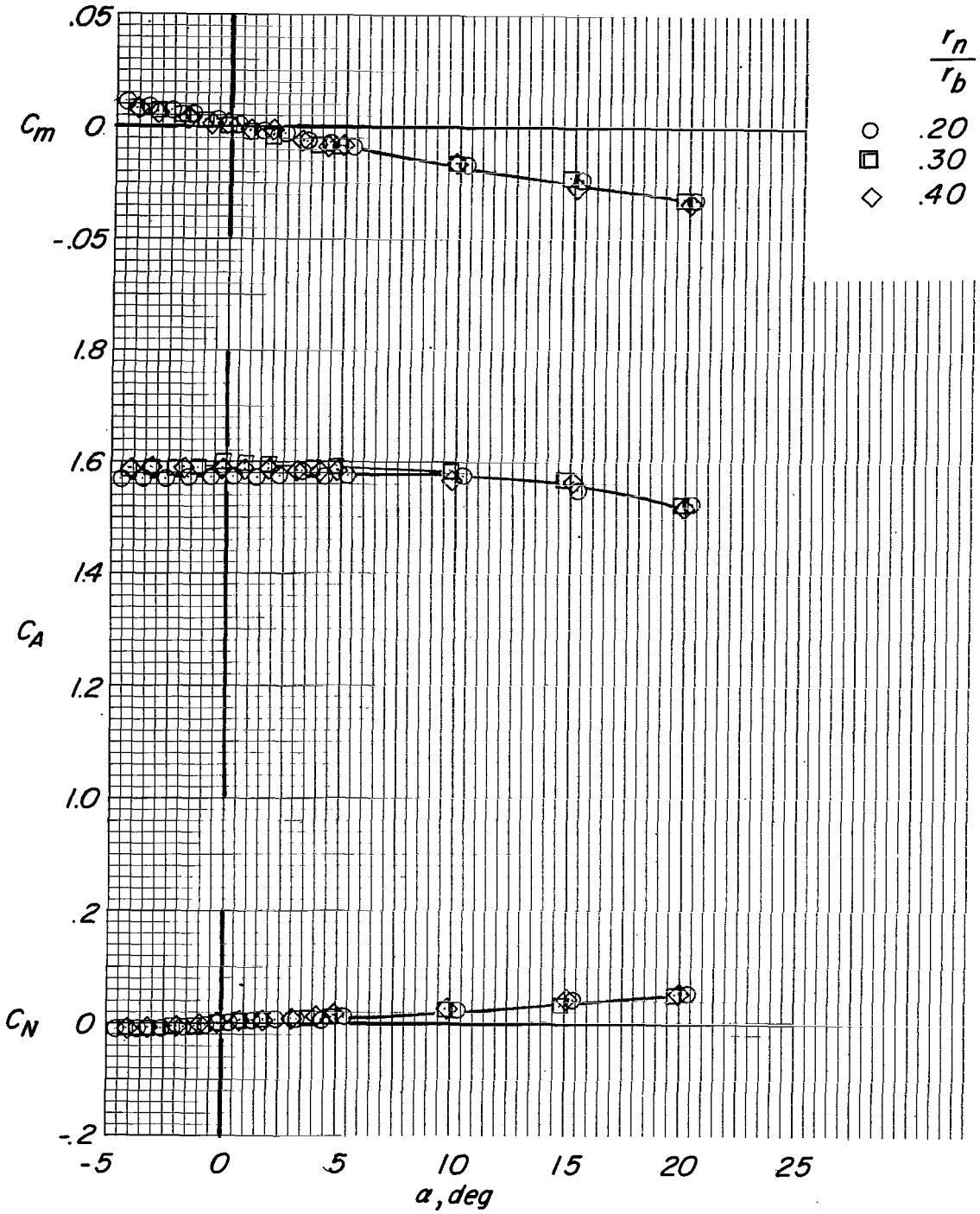

(a) M = 2.30; R = 0.73 × 10^6.

Figure 7.- Effect of nose radius on static longitudinal aerodynamic characteristics of tension shells. A^2 = 0.833.

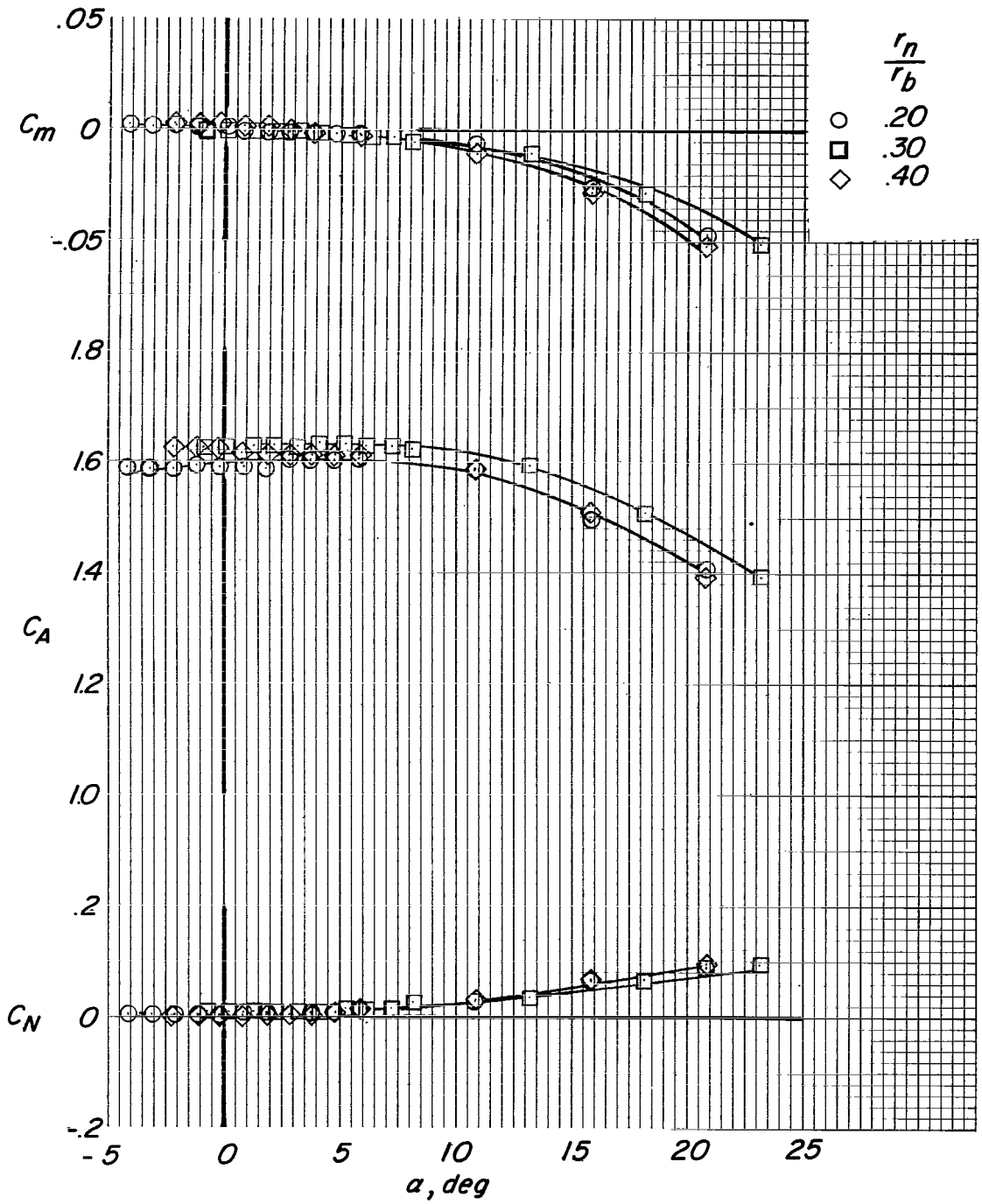

(b) M = 4.63; R = 0.73 × 10^6.

Figure 7.- Continued.

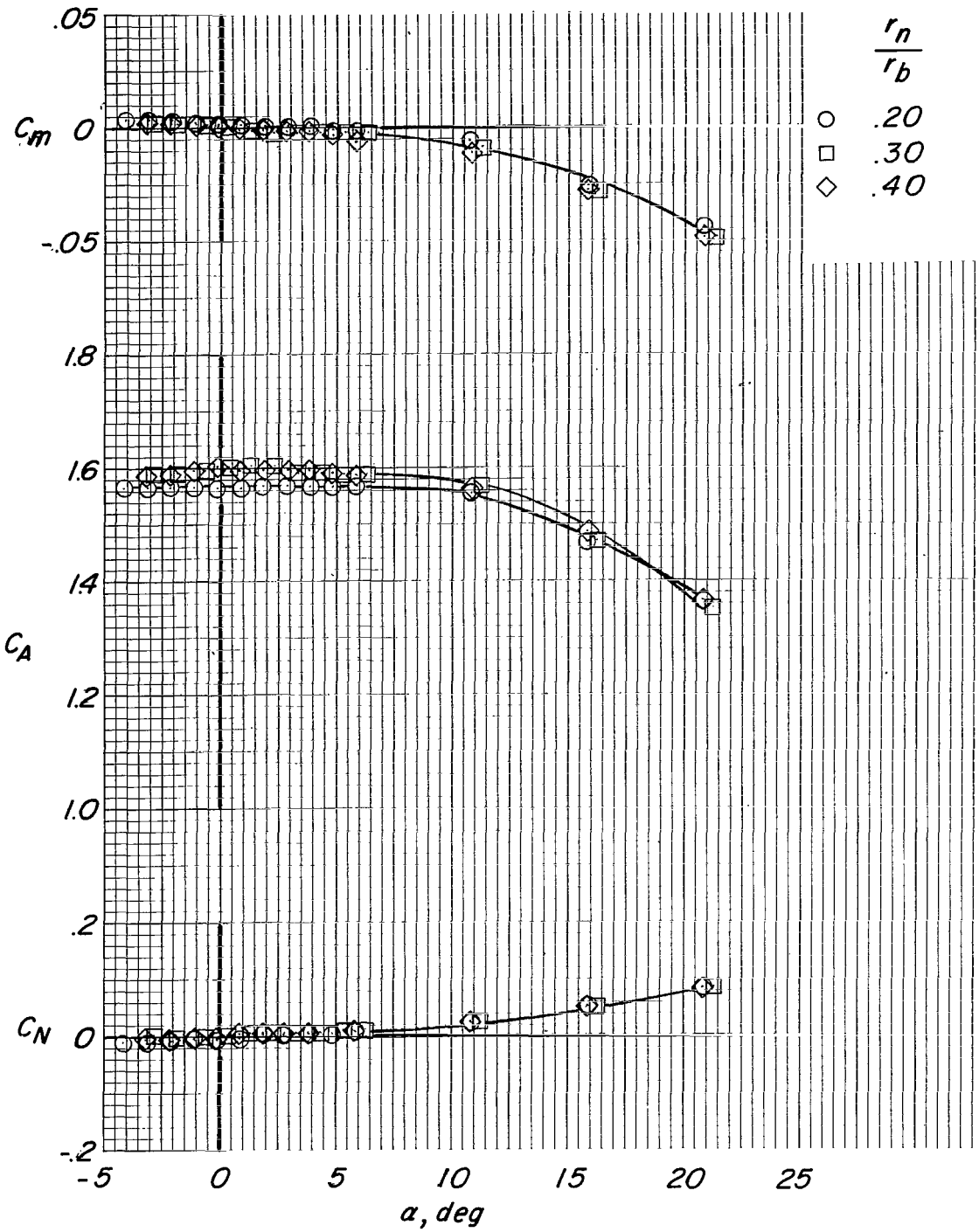

(c) M = 4.63; R = 2.01×10^6.

Figure 7.- Concluded.

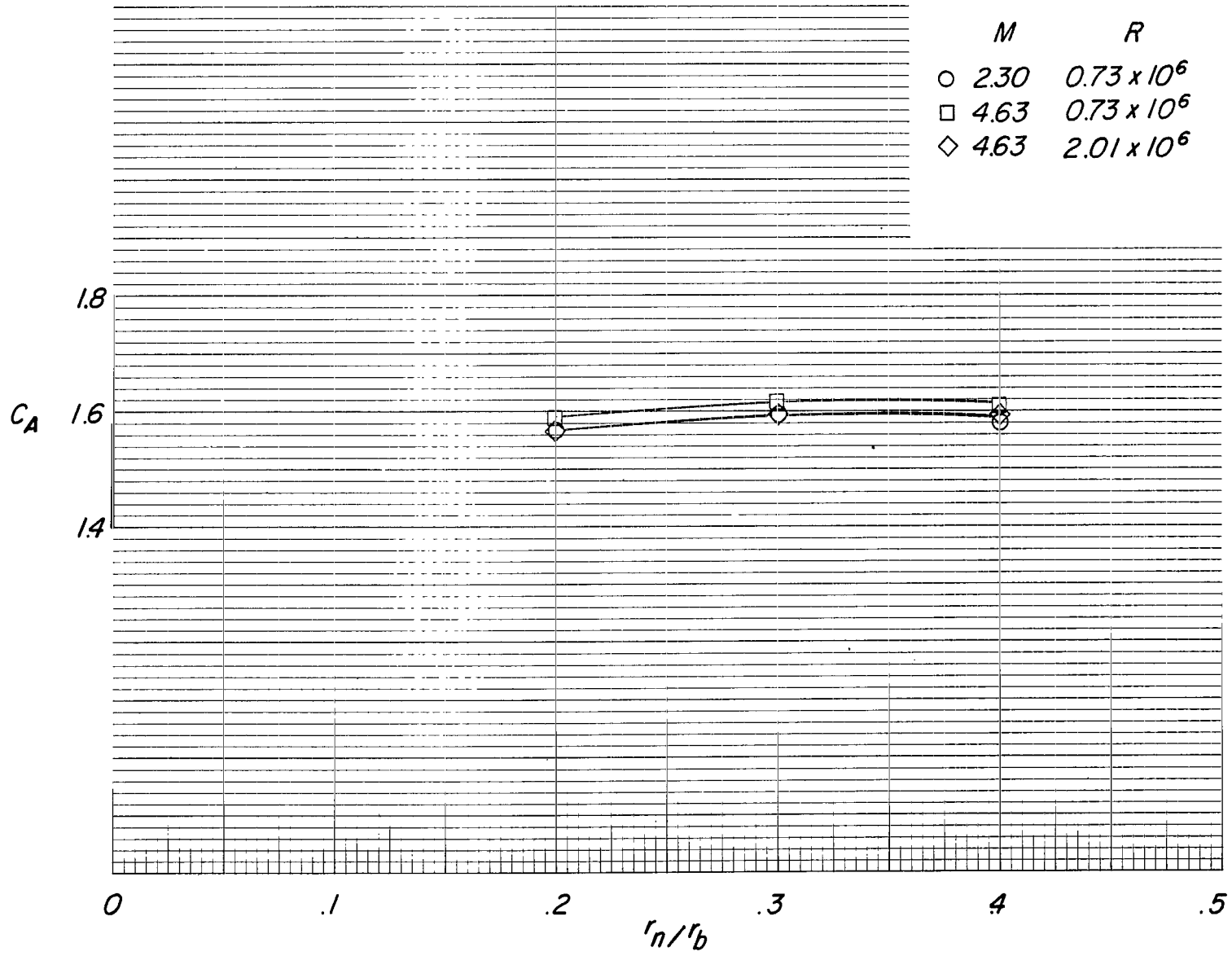

Figure 8.- Summary of axial-force coefficients at $\alpha \approx 0^0$ of tension shells.

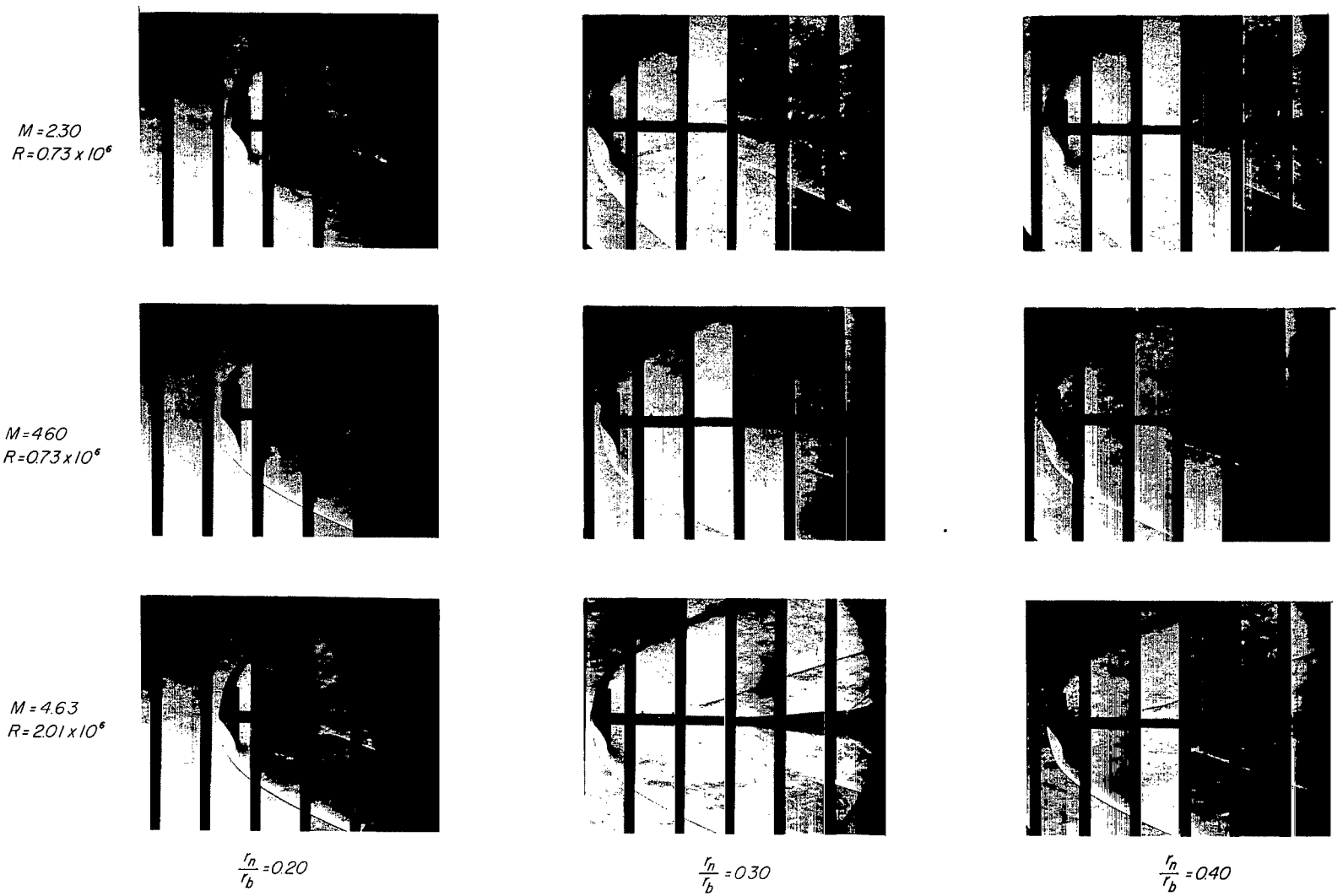

Figure 9.- Schlieren photographs of tension shells ($A^2 = 0.833$). $\alpha \approx 0^0$; $\frac{r_s}{r_b} = 0.05$.

L-69-1305

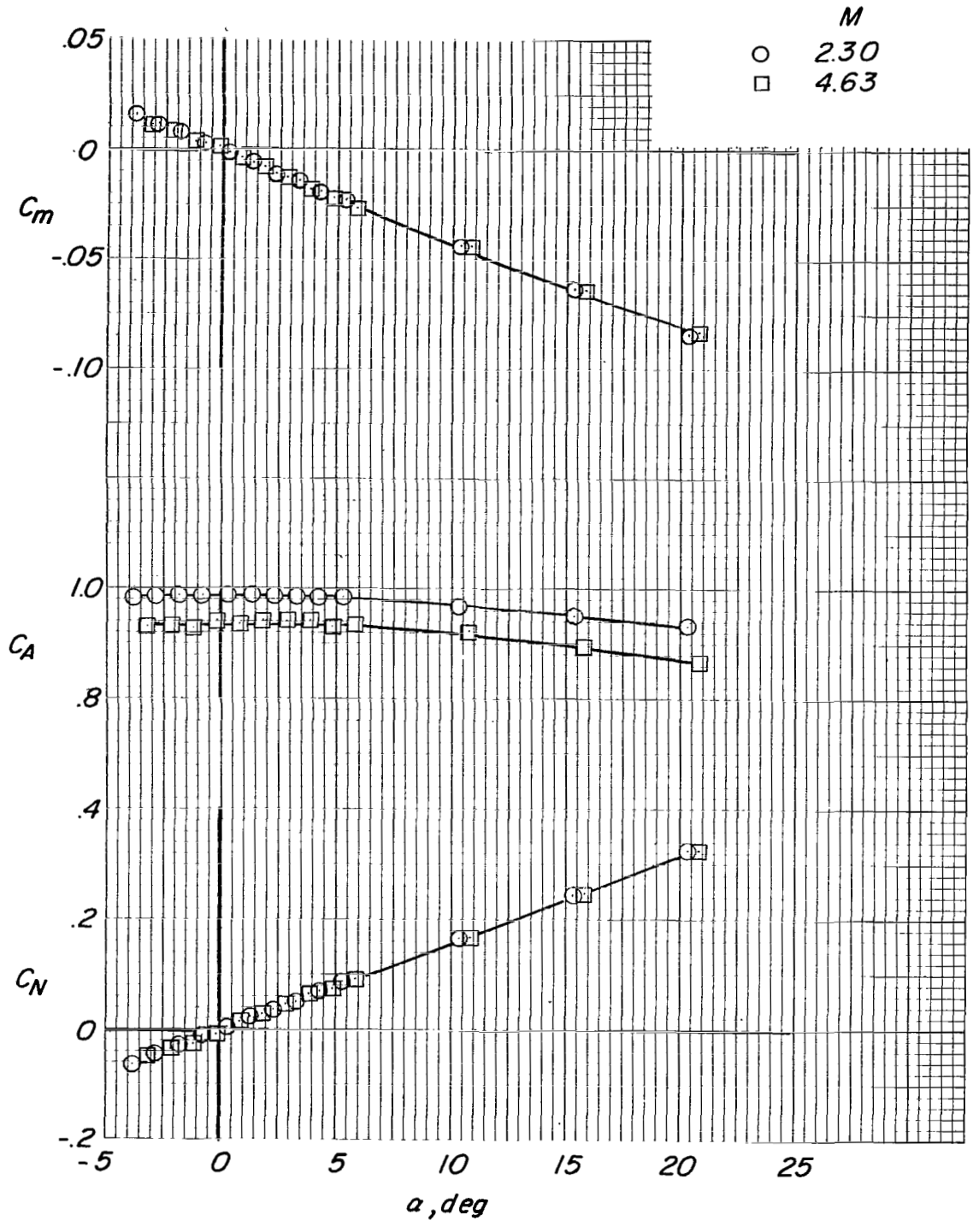

Figure 10.- Static longitudinal aerodynamic characteristics of an attached inflatable decelerator. $R = 0.73 \times 10^6$.

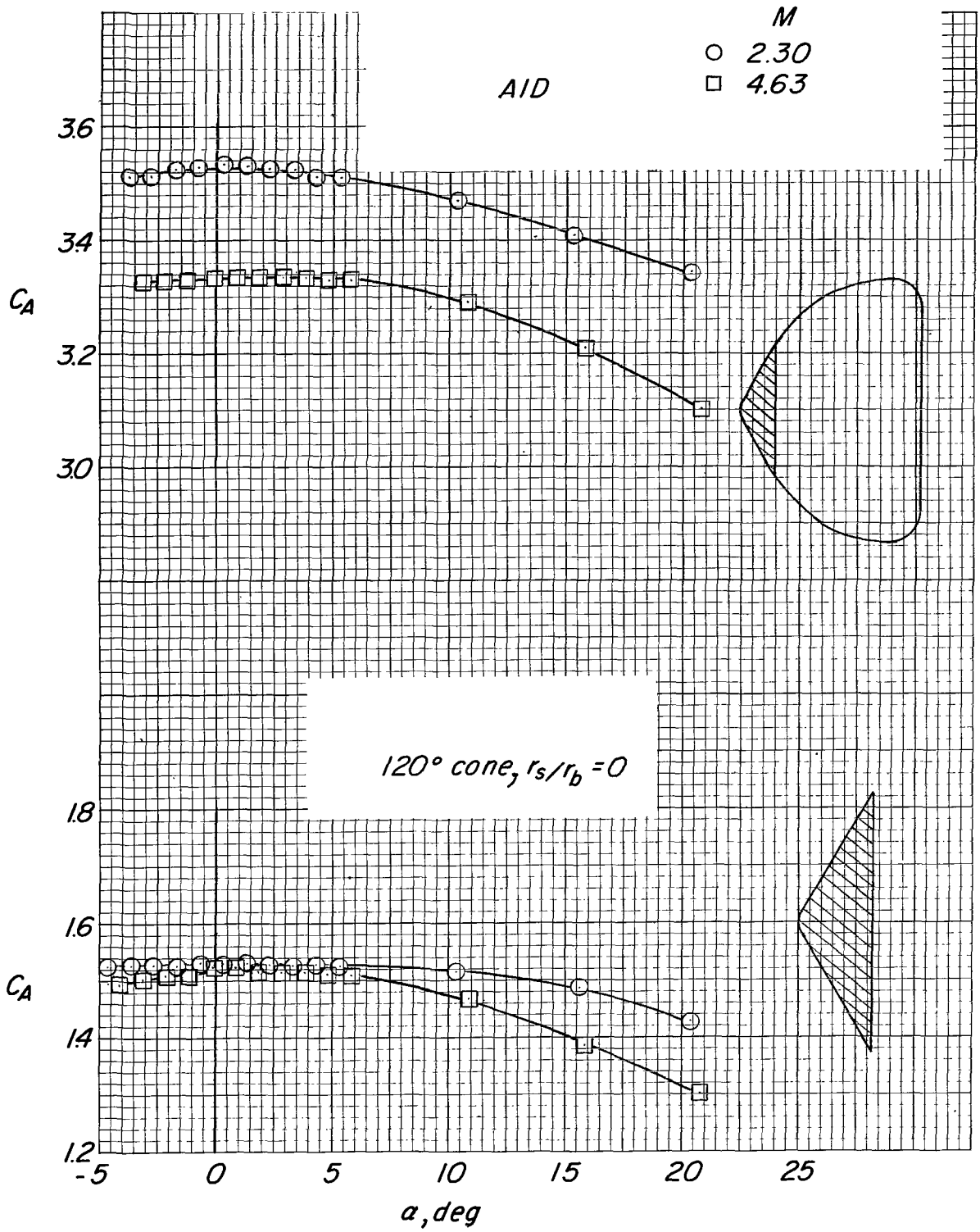

Figure 11.- Axial-force coefficients for AID and sharp-shoulder cone.

NASA-Langley, 1969 —— 31 L-6427

"The aeronautical and space activities of the United States shall be conducted so as to contribute . . . to the expansion of human knowledge of phenomena in the atmosphere and space. The Administration shall provide for the widest practicable and appropriate dissemination of information concerning its activities and the results thereof."

—NATIONAL AERONAUTICS AND SPACE ACT OF 1958

NASA SCIENTIFIC AND TECHNICAL PUBLICATIONS

TECHNICAL REPORTS: Scientific and technical information considered important, complete, and a lasting contribution to existing knowledge.

TECHNICAL NOTES: Information less broad in scope but nevertheless of importance as a contribution to existing knowledge.

TECHNICAL MEMORANDUMS: Information receiving limited distribution because of preliminary data, security classification, or other reasons.

CONTRACTOR REPORTS: Scientific and technical information generated under a NASA contract or grant and considered an important contribution to existing knowledge.

TECHNICAL TRANSLATIONS: Information published in a foreign language considered to merit NASA distribution in English.

SPECIAL PUBLICATIONS: Information derived from or of value to NASA activities. Publications include conference proceedings, monographs, data compilations, handbooks, sourcebooks, and special bibliographies.

TECHNOLOGY UTILIZATION PUBLICATIONS: Information on technology used by NASA that may be of particular interest in commercial and other non-aerospace applications. Publications include Tech Briefs, Technology Utilization Reports and Notes, and Technology Surveys.

Details on the availability of these publications may be obtained from:

SCIENTIFIC AND TECHNICAL INFORMATION DIVISION

NATIONAL AERONAUTICS AND SPACE ADMINISTRATION

Washington, D.C. 20546